國立交通大學

機械工程研究所

碩士論文

化學機械平坦化之最佳化操作：
動態規劃法

Optimal Operation of
Chemical Mechanical Planarization：
Dynamic Programming Approach

研究生:李永洲
指導教授:林家瑞 博士

中華民國九十三年六月

化學機械平坦化之最佳化操作：動態規劃法

Optimal Operation of Chemical Mechanical Planarization：Dynamic Programming Approach

研究生：李永洲　　Student：Young-Chou Lee

指導教授：林家瑞　　Advisor：Dr. Chia-Shui Lin

國立交通大學

機械工程研究所

碩士論文

A Thesis
Submitted to Institute of Mechanical Engineering
College of Engineering
National Chiao-Tung University
in Partial Fulfillment of the Requirements
for the Degree of
Master of Science
In
Mechanical Engineering
June 2004
Hsinchu, Taiwan, Republic of China

中華民國九十三年六月

化學機械平坦化之最佳化操作：

動態規劃法

學生：李永洲　　　　　　　　　　　　　　　　　　指導教授：林家瑞　博士

國立交通大學機械工程研究所

碩士論文

摘要

在本論文中，我們探討在一片二氧化矽或銅晶圓的研磨過程中，改變向下壓力與旋轉速度對不平坦度的影響。因為向下壓力與旋轉速度的大小皆有其限制的範圍，我們運用動態規劃設計有限向下壓力及旋轉速度的化學機械研磨之最佳化操作，並藉由更精確描述化學機械研磨的模型，在其他參數皆為固定的條件下，計算出輸入的改變量與時間，接著將最佳化計算結果在控片上作實驗，並與傳統的固定移除率操作方法作比較。此外，在有圖案的銅晶圓研磨，運用高處所受的向下壓力比低處高的假設，建立階梯高度的模型，並藉由模擬的結果說明向下壓力對平坦化效率的影響。

Optimal Operation of Chemical Mechanical Planarization：Dynamic Programming Approach

Student：Young-Chou Lee　　　　　　　　Advisor：Dr. Chia-Shui Lin

Institute of Mechanical Engineering

National Chiao Tung University

Abstract

In this thesis, the impact on non-planarization index by the down force and rotational speed during a SiO_2 or Cu CMP process was investigated. Since the magnitudes of down force and rotational speed have limits, we choose the dynamic programming approach because of its ability to achieve constrained optimization by the down force and rotational speed. The duration and the amount of input were computed based on the more accurate chemical mechanical polishing model when the other parameters were fixed. Experiments based on dynamic programming were done for blanket wafers and the conventional operation was compared with the dynamic programming operation. Besides, the model for the step height reduction was established in the case of pattern wafer. The model was based on the assumption that at the feature scale, high areas on the wafer experience higher pressure than the lower areas. The influence of the planarization efficiency by the down force was discussed based on the simulation result.

誌謝

感謝指導教授林家瑞博士兩年來細心與耐心的指導，讓我在碩士生涯中學習到如何做研究的方法，使我能掌握研究的方向，更重要的是學習到做人處世的原則。另外也感謝林仁輝博士與陳宗麟博士在論文口試時惠予的建議與指導，並感謝賴明志工程師對實驗上的協助，有各位的寶貴意見使我終於順利完成論文，非常感謝各位。

在研究所的生活中，很幸運的能有建宇、朝雯、介民與木坤在一起打拼、一起打球、游泳與聊天，讓我的研究所生活增添許多樂趣，也更加充實與豐富，並感謝研究所認識的同學們，使生活充滿歡笑與快樂。

最後，感謝家人的支持與鼓勵，使我無顧慮與專心的在學業上努力，也感謝女友的關心與包容。在此，僅將此論文獻給我最親愛的父母。

Contents

Chinese Abstract…………………………………………………………………...I

English Abstract…………………………………………………………………...II

Acknowledgement…………………………………………………………………...III

List of Tables…………………………………………………………………...VI

List of Figures…………………………………………………………………..VIII

Chapter 1 Introduction………………………………………………………………1

1.1 Literature Survey and Motivation……………………………………………………1

1.2 Thesis Outline…………………………………………………………………..3

Chapter 2 An Overview of CMP Process and Model Representation…………….5

2.1 Introduction of CMP Structure………………………………………………….....5

2.2 CMP Process Parameters…………………………………………………………..7

2.2.1 Mechanical Parameters…………………………………………………………7

2.2.2 Chemical Parameters…………………………………………………………...8

2.3 Model of Chemical Mechanical Polishing………………………………………..10

2.3.1 Preston Equation……………………………………………………………....11

2.3.2 Luo and Dornfeld Equation……………………………………………………11

Chapter 3 Optimal Control Design：Dynamic Programming…………………....13

3.1 Bellman's Principle of Optimality………………………………………………...13

3.2 Dynamic Programming…………………………………………………………...14

3.3 Simulation Results………………………………………………………………...16

3.3.1 SiO_2 CMP Process…………………………………………………………..18

3.3.2 Cu CMP Process………………………………………………………………20

3.4 Discussion and Summary………………………………………………………....23

Chapter 4 Experiment and Discussion for SiO_2 and Cu Blanket Wafer………....25

4.1 CMP Process for Experiment……………………………………………………..25

4.1.1 Sample Preparation……………………………………………………...25
4.1.2 Post CMP Cleaning……………………………………………………...26
4.1.3 Static Etching Experiment………………………………………………26
4.2 Evaluation of CMP Performance…………………………………………...27
4.2.1 SiO_2 and Cu Film Thickness Determination……………………………27
4.2.2 CMP Removal Rate and Non-Planarization Index………………………27
4.3 SiO_2 CMP Experiment…………………………………………………...28
4.3.1 Change Down Force as the Admissible Input…………………………...28
4.3.2 Change Rotational Speed as the Admissible Input………………………29
4.3.3 Change Down Force and Rotational Speed as the Admissible Inputs Simultaneously…………………………………………………………..29
4.4 Cu CMP Experiment……………………………………………………...29
4.4.1 Change Down Force as the Admissible Input…………………………...30
4.4.2 Change Rotational Speed as the Admissible Input………………………30
4.4.3 Change Down Force and Rotational Speed as the Admissible Inputs Simultaneously…………………………………………………………31
4.5 Discussion and Summary……………………………………………………...31
Chapter 5 Pattern Copper Wafer…………………………………………………34
5.1 Introduction……………………………………………………………………34
5.2 Model development……………………………………………………………35
5.3 Simulation……………………………………………………………………..37
5.4 Discussion and Summary……………………………………………………...39
Chapter 6 Conclusion and Future Work………………………………………..40
Reference……………………………………………………………………………79

List of Tables

Table 2-1 The Parameters of CMP Process……………………………………...41

Table 3-1 Process Parameters of SiO_2 CMP Experiment…………………………..42

Table 3-2 Slurry Formulation of SiO_2 CMP………………………………………43

Table 3-3 The Experimental Results of SiO_2 CMP to Determine C_1 and C_2………43

Table 3-4 The Experiment Data of SiO_2 CMP……………………………………..43

Table 3-5 The Values of Admissible Inputs by Corresponding Down Force………43

Table 3-6 The Result of Dynamic Programming of SiO_2 CMP with Down Force...44

Table 3-7 The Values of Admissible Inputs by Corresponding Rotational Speed ……………………………………………………………………..44

Table 3-8 The Result of Dynamic Programming of SiO_2 CMP with Rotational Speed……………………………………………………………………44

Table 3-9 The Result of Dynamic Programming of SiO_2 CMP with Two Inputs….44

Table 3-10 Process Parameters of Cu CMP Experiment…………………………...45

Table 3-11 Slurry Formulation of Cu CMP………………………………………...45

Table 3-12 The Experimental Results of Cu CMP to Determine C_1 and C_2………46

Table 3-13 The Experiment Data of Cu CMP……………………………………...46

Table 3-14 The Values of Admissible Inputs by Corresponding Down Force…......46

Table 3-15 The Result of Dynamic Programming of Cu CMP with Down Force…46

Table 3-16 The Values of Admissible Inputs by Corresponding Rotational Speed ……………………………………………………………………47

Table 3-17 The Result of Dynamic Programming of Cu CMP with Rotational Speed ……………………………………………………………………47

Table 3-18 The Result of Dynamic Programming of Cu CMP with Two Inputs…..47

Table 4.1 SiO_2 Blanket Wafer Experimental Result by Down Force with Dynamic Programming……48
Table 4.2 SiO_2 Blanket Wafer Experimental Result by Down Force with Constant Removal Rate……48
Table 4.3 SiO_2 Blanket Wafer Experimental Result by Rotational Speed with Dynamic Programming……49
Table 4.4 SiO_2 Blanket Wafer Experimental Result by Rotational Speed with Constant Removal Rate……49
Table 4.5 SiO_2 Blanket Wafer Experimental Result by Two Admissible Inputs with Dynamic Programming……50
Table 4.6 SiO_2 Blanket Wafer Experimental Result by Two Admissible Inputs with Constant Removal Rate……50
Table 4.7 Cu Blanket Wafer Experimental Result by Down Force with Dynamic Programming……51
Table 4.8 Cu Blanket Wafer Experimental Result by Down Force with Constant Removal Rate……51
Table 4.9 Cu Blanket Wafer Experimental Result by Rotational Speed with Dynamic Programming……52
Table 4.10 Cu Blanket Wafer Experimental Result by Rotational Speed with Constant Removal Rate……52
Table 4.11 Cu Blanket Wafer Experimental Result by Two Admissible Inputs with Dynamic Programming……53
Table 4.12 Cu Blanket Wafer Experimental Result by Two Admissible Inputs with Constant Removal Rate……53
Table 4.13 Comparison of Non-Planarization Index (SiO_2 Blanket Wafer)……54
Table 4.14 Comparison of Non-Planarization Index (Cu Blanket Wafer)……54

List of Figures

Figure 1.1 Schematics of a Single Layer Cu Interconnect： (a) Before Polishing (b) Ideal Case After Polishing and (c) Real Case After Polishing…………55

Figure 1.2 (a) Dependence of Copper Dishing and Oxide Erosion on Platen Speed. Wafer Pressure was Kept Constant. [10]………………………………56

Figure 1.2 (b) Dependence of Copper Dishing and Oxide Erosion on Wafer Pressure. Platen Speed was Held Constant. [10]…………………………………56

Figure 1.3 Trajectory for RR_{max}=9000 Å/min, u_{max}=360000 Å/min^2, H_{small}=2000 Å, and RR_{small}=2000 Å/min [9]……………………………………………57

Figure 2.1 The Mimic Schematic of CMP…………………………………………58

Figure 2.2 CMP Motion……………………………………………………………58

Figure 2.3 The Perspective Front-View of CMP System- Westech 372M Machine ……………………………………………………………………………...59

Figure 2.4 The Removal Rate Curves for Pad with Conditioning and without Conditioning [8]…………………………………………………………...60

Figure 2.5 The Removal Rate Curve for Platen Speed [16]………………………..60

Figure 2.6 The Removal Rate Curve for Down Force [16]………………………...61

Figure 2.7 MRR as a Function of Abrasive Size Distribution and Abrasive Weight Concentration [11]……………………………………………………....61

Figure 2.8 Effects of Oxidizer Concentration on Removal Rate [12]……………...62

Figure 2.9 Two Contact Modes of CMP：(a) Hydro-Dynamic Contact Mode and (b) Solid-Solid Contact Mode [8]…………………………………………..62

Figure 3.1 Illustration of the Principle of Optimality………………………………63

Figure 3.2 Complete Result of Dynamic Programming and Recovery of the Optimal Trajectory from Initial State x(0)………………………………………63

Figure 3.3 A Controller Based on Retrieving the Results of the Dynamic Programming Computation from Memory……………………………..64
Figure 3.4 Program Flowchart of Dynamic Programming…………………………65
Figure 3.5 The Model Prediction and Experimental Observations of the Effects of the Down Force and Rotational Speed for SiO_2 Blanket Wafer………..66
Figure 3.6 The Simulation Result of SiO_2 Blanket Wafer when the Down Force as the Variable Input……………………………………………………67
Figure 3.7 The Simulation Result of SiO_2 Blanket Wafer when the Rotational Speed as the Variable Input…………………………………………………68
Figure 3.8 The Simulation Result of SiO_2 Blanket Wafer when the Rotational Speed and Down Force as the Variable Inputs Simultaneously………………..69
Figure 3.9 The Model Prediction and Experimental Observations of the Effects of the Down Force and Rotational Speed for Cu Blanket Wafer…………70
Figure 3.10 The Simulation Result of Cu Blanket Wafer when the Down Force as the Variable Input…………………………………………………...71
Figure 3.11 The Simulation Result of Cu Blanket Wafer when the Rotational Speed as the Variable Input……………………………………………...72
Figure 3.12 The Simulation Result of Cu Blanket Wafer when the Rotational Speed and Down Force as the Variable Inputs Simultaneously………………73
Figure 4.1 (a) The Structure of SiO_2 Blanket Wafer (b) the Structure of Cu Blanket Wafer…………………………………………………………………...74
Figure 4.2 The Assembly of the Experiment for Static Etching [16]………………75
Figure 4.3 9 Points of Thickness Measurement……………………………………75
Figure 5.1 Typical Three-Step Procedure in Cu CMP: Planarization, Planarization/Overpolish, and Overpolish [28]………………………...76

Figure 5.2 Schematic Picture of the Model……………………………………...76
Figure 5.3 Comparison between Luo and Dornfeld Equation and Power Function Fit for Experimental Cu Blanket Wafer Removal Rate……………………77
Figure 5.4 Model Prediction Compared with Experimental Data from Stavreva [22] for Step Height versus Polishing Time…………………………………78
Figure 5.5 Planarization Efficiency versus Down Force…………………………...78

Chapter 1

Introduction

The chemical mechanical polishing (CMP) process removes material from the wafer surface through both physical friction and chemical etch. CMP has been shown to be the only technology capable of achieving planarization on the global scale in the integrated circuits (IC) industry. CMP was developed at IBM^{TM} during the early 1980s. At that time, multilevel interconnect technology was being pushed to the limits of circuit density and performance. This technique which helps improve both photolithography and deposition process solved this problem. CMP produces excellent planarization across the wafer surface as well as lessening the effects of existing surface defects and has the benefit of repeatable process, compatible with all device types and generations. Therefore, many semiconductor manufactures have been developing CMP process with all their strength in order to get an advantageous position in the IC industry.

1.1 Literature Survey and Motivation

The interlayer dielectric (ILD) film has surface ridges that reflect the underlying metal interconnection patterns. In deep submicron photolithography, on the other hand, the margin of depth of focus is reduced to a submicron range, and the submicron-height surface ridges cause local defects in the photoresist pattern. That is, interlayer dielectric planarization has become more critical as the number of metal stack layers has increased [1]. In addition, higher operating frequencies for IC chips lead to higher current densities in smaller features of interconnection. As a result, a

highly reliable metal line which allows high current density is necessary [2]. Copper has emerged as the optimal interconnect material because of its lower electrical resistivity and better resistance to electromigration compared to aluminum. Patterned Cu lines are produced by a damascene process. In the damascene process, the dielectric is patterned, followed by the barrier and metal deposition. The barrier becomes necessary when using Cu as an interconnect material to prevent the rapid diffusion of the Cu into the dielectric. The final step in this process is CMP that removes the excess metal and provides global planarization. Fig. 1.1 schematically shows a single layer Cu interconnect structure before and after CMP. Two key problems in Cu pattern wafer CMP, namely copper dishing and oxide erosion, generate surface non-planarity which gives rise to issues with integrating multiple layers of metal. Copper and oxide thinning results in increased RC delay leading to inferior device performance. Therefore, we focus on the experiments for SiO_2 and Cu CMP.

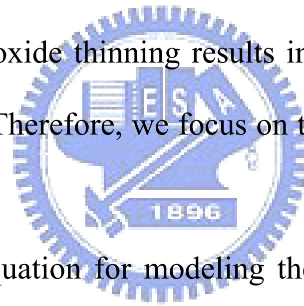

The most well known equation for modeling the CMP process is the Preston's equation [3]. Preston's equation reflects the influence of process parameters including down force and relative velocity. In the last several years, the revised Preston's equations concentrated on different elements of CMP. For example, Zhang and Busnaina [4] proposed an equation taking into account the normal stress and shear stress acting on the contact area between abrasive particles and wafer surfaces. Tseng and Wang [5] showed that the removal rate is proportional to the terms $P^{5/6}$ and $V^{1/2}$. Zhao and Shi [6], [7] consider the effects of the pad hardness and the contact between wafer and pad. However, most of the models are quite rough. Luo and Dornfeld [8] assumed an indentation-sliding model for the penetration of the pad and included an empirical accommodation of chemical reaction at the wafer surface. Compared with experiment results, the model accurately predicts the removal rate. Therefore, we used

the model to predict the removal rate in the dynamic programming approach.

Jian-Bin Chiu and Cheng-Ching Yu etc. [9] used the concept of soft landing of a spacecraft to CMP operation. Therefore, the CMP operation can be formulated as a minimum time optimal control problem. They treat the oxide surface as the landing surface, the polishing pad as a fly vehicle, and the removal rate as the vertical velocity. The equations describing the removal can be expressed as：

$$\begin{bmatrix} \dot{H} \\ \dot{RR} \end{bmatrix} = \begin{bmatrix} 0 & -1 \\ 0 & 0 \end{bmatrix} \begin{bmatrix} H \\ RR \end{bmatrix} + \begin{bmatrix} 0 \\ 1 \end{bmatrix} u$$

$$-u_{max} \le u \le u_{max}$$

where H is the thickness of material to be removed, RR the removal rate, and u the rate of change of the removal rate. The constraints in removal rate and rate of change of removal rate are applied because the parameters of CMP machine have physical limit, e.g. platen speed, down force, and slurry flow rate. They also set the final condition to $H(t_f)$ =2000Å and $RR(t_f)$ =2000 Å/min in order to reduce the dishing and erosion according to the experimental data proposed by K. Wijekoon and S. Tsai etc. [10]. Fig. 1.2 shows the dishing and erosion are proportional to the pressure and relative velocity. Once the landing point is reached ($H(t_f)$ =2000Å), the polisher continues the removal with the smaller removal ($RR(t_f)$ =2000 Å/min) until the end point is detected. Fig. 1.3 shows the result of optimal operation. Through their inspiration, we plan to use dynamic programming as our method of optimal operation in this thesis.

1.2 Thesis Outline

In this study, we focus on the mechanical effects in CMP. The down force and rotational speed were taken to be the operational parameters. In chapter 2, an

overview of the CMP process and the parameters of mechanical and chemical aspects were introduced and the model which was used in simulation was represented. In chapter 3, the method of dynamic programming was introduced and the simulation data were discussed. In chapter 4, the experimental results through the operation of dynamic programming were obtained and the result was discussed. In chapter 5, we focus on the step height reduction by the down force based on the force redistribution. The simulation data were presented. Finally, the conclusion and future work were presented in chapter 6.

Chapter 2

An Overview of CMP Process and Model Representation

CMP has been used to polish a variety of material for thousands of year, for example to produce optically flat and mirror finished surface. More recently optically flat and damage-free glass and semiconductor surfaces have been prepared by use of the CMP processes. Now CMP is being introduced in planarizing the interlayer dielectric and metal wiring to form interconnections between device and device.

2.1 Introduction of CMP structure

A schematic of a CMP machine and the perspective front-view of a typical CMP system are shown in Fig. 2.1, 2.2 and 2.3. Both the carrier and pad are rotated in the same direction with different velocities. The flowing slurry is carried onto the wafer surface through the porosity on the pad surface. The slurry chemically attacks and softens the wafer surface, which is then removed by mechanical abrasion. The primary segments of CMP machine are as follows：

(1) Wafer Carrier：

The wafer carrier holds the wafer face down during CMP and brings the wafer in contact with the polishing pad. The carrier rotates in the same direction as the platen.

(2) Platen：

The rotating base on which the polishing pads are placed. Sometimes referred

to as the polishing “table”.

(3) Polish Arm：

Transport the wafer by the polish arm.

(4) Pad：

A pad which is mounted on a rotating platen and polishes the wafer. Polishing pads come in a variety of materials and are designed with a variety of surface features depending on the process results needed.

(5) Slurry：

An abrasive mixture containing particles of colloidal silica, alumina, or some other abrasive material suspended in a chemical compound and DI water. Slurry is fed onto and through the polishing pad during CMP in order to remove material from the wafer surface.

(6) Pad Conditioning：

A process in which the polishing pad is “roughed up” by a diamond disc in order to reduce the effects of glazing. In Fig. 2.4, conditioning enhances pad performance, but reduces overall pad lifetime.

If we only care about the amount of mechanical abrasion, it will result in a decreased removal rate and the wafer surface may peel off or be scratched. On the other hand, if we only care abut the amount of chemical reaction removal, it will lead to the erosion of the dielectric or the dishing of the metal lines. Giving undue emphasis to either of them will not achieve the global planarization. Therefore, how

to combine the mechanical abrasion and chemical reaction to get good performance and high throughput is nowadays an important challenge to be dealt with.

2.2 CMP Process Parameters

As named chemical mechanical polishing, the primary parameters are divided into two parts which are the chemical aspect and the mechanical aspect.

2.2.1 Mechanical Parameters

The primary mechanical parameters are as follows：

(1) Platen Speed：

The platen speed affects slurry transport across the wafer and the transport of the reactions and products of chemical reactions to and from the wafer surface. It has been noted that the copper removal rate is strongly dependent on the platen speed. In Fig. 2.5 [16], as the platen speed increases, the removal rate increases.

(2) Carrier Speed：

When the carrier speed is the same as the platen speed, the best uniformity will be achieved.

(3) Down Force：

In Fig. 2.6 [16], as the down force increases, the removal rate increases and then reduces the polishing time. This, of course, means higher throughput. The danger is that too much down force can cause problems such as scratches or gouges, and can possibly cause non-uniformity.

(4) Back Pressure：

It is sometimes used to provide some curvature or shape to the wafer during polishing. The idea is to produce an optimum wafer shape with respect to the pad underneath for improving removal rate distribution on the wafer and within-wafer-uniformity (WIWUN).

(5) Pad Conditioning：

There are variables which will affect pad conditioning. For instance, the conditioning duration, the abrasiveness of the disc and down force will all have an effect on the pad. A long conditioning duration may improve pad performance, but ultimately will reduce pad lifetime.

(6) Slurry Flow Rate：

Slurry flow rate affects how quickly new chemicals and abrasive are delivered to the pad and reaction by-products and used abrasive are removed from pad. It also affects how much slurry is on the pad and therefore will affect the lubrication properties of the system.

Furthermore, there are still other mechanical parameters which affect the process：polish oscillation, wafer mounting and pad hardness, for instance.

2.2.2 Chemical Parameters

The primary chemical parameters are as follows：

(1) Abrasive Size

Abrasive size affects the removal rate and the surface damage. For example,

experimental results show that there is an inverse proportional relationship between the abrasive size and the material removal rate, Fig. 2.7 [11].

(2) Abrasive Weight Concentration

Abrasive weight concentration also affects the removal rate. For instance, experimental results show that there is a proportional relationship between the abrasive concentration and the material removal rate, Fig. 2.7 [11].

(3) Abrasive Variety

Silica oxide (SiO_2) is the most common used for oxide polishing while aluminum oxide (Al_2O_3) is the most common used for metal polishing.

(4) Slurry Viscosity

The more viscous a material, the more it resists flow. High slurry viscosity results in poor transport of reactants and products to and from the wafer surface. It also affects lubrication of the wafer pad interface.

(5) Oxidizer Concentration

In Fig. 2.8 [12], at the region of low oxidizer concentration, the rate of oxide generation is small and the passivation layer is removed as soon as it is formed. Then a maximal removal rate is reached when the rate of passivation is equal to the rate of mechanical abrasion. As we increase the oxide concentration further, the passivation itself changes its structure. This creates a barrier for mechanical abrasion and slows down the removal rate.

Furthermore, there are still other chemical parameters which affect the process：

slurry temperature, slurry buffering and film hardness, for instance.

There are many variables that can affect the CMP performance as shown in Table 2-1. Besides, some factors which are difficult to control and monitor like the slurry transport under the wafer and the local temperature of the slurry also have significant effects on the CMP performance and the process parameters are interrelated such that modifications to one parameter will have an impact on other process issues. For instance, increasing platen speed or down force may increase the removal rate, yet at the same time create slurry flow rate and distribution problems. Therefore, the key problem is how to optimize the process parameter settings in order to obtain the desired results for the given film being planarized.

2.3 Model of Chemical Mechanical Polishing

The material removal model for CMP can be separated into two parts, mechanical model and chemical model. The chemical action of the slurry is responsible for continuously softening the silicon oxide or oxidizing the metal surface to form a thin passive layer which is immediately removed by the action of the slurry abrasives. The fresh silicon oxide or metal surface exposed due to the abrasion is then rapidly repassivated and removed. This process of passivation-abrasion-repassivation continuous until the desired thickness is realized. Based on this idea, a mechanical removal model and a chemical model can be independently developed for CMP, with the mechanical model considering only the mechanical removal of the passivation layer, and the chemical model considering only the passivation of this layer.

2.3.1 Preston Equation

Preston provided a simple model of material removal in glass polishing tools, postulated based on experimental observation that the removal rate is proportional to the nominal applied pressure and the relative velocity between the pad and the material being polished. Preston equation [3] for the removal rate RR can be written as

$$RR = K_p P V$$

where P is the down pressure, V the relative velocity of wafer, and K_p a constant representing the effect of other remaining parameters, such as the abrasive type and concentration, and the nature of the chemicals and their concentrations. This equation has been widely used in CMP process control and consumable development for IC fabrication and manufacturing. However, it is focused on mechanical removal of material and there are some other phenomenons that can not be explained. For example, experimental results show that the pressure dependence of removal rate for CMP with soft pad satisfies a nonlinear relationship. Therefore, what is included in the all-purpose parameter K_p is unclear.

2.3.2 Luo and Dornfeld Equation

Luo and Dornfeld proposed a model to describe the interactions between the wafer, pad, and abrasives, which are quite different from those in conventional polishing or lapping processes due to the small pad hardness and different size scales of the pad asperity and the polishing abrasives. They assumed the removal mechanism in the solid-solid contact mode instead of the hydro-dynamic mode, as shown in Fig. 2.9. Luo and Dornfeld equation [8] for the removal rate RR can be written as

$$RR = C_2\left(1-\Phi\left[3-C_1P_0^{1/3}\right]\right)\sqrt{P_0}V + RR_C$$

where P_0 is the down pressure

V is the relative velocity of wafer

C_1 is a constant representing the effect of slurry abrasives (average size and size distribution), wafer and pad hardness, and pad roughness

C_2 is a constant representing the effect of slurry chemicals, slurry abrasives, wafer size, wafer density, wafer hardness, pad material, and pad roughness

Φ is the normal cumulative distribution function which representing the probability density of active abrasives over the wafer-pad interface

$$\Phi(x) = \frac{1}{\sqrt{2\pi}}\int_{-\infty}^{x} e^{-(1/2)t^2}dt$$

RR_C is the material removal due to chemical etch

The values, C_1 and C_2, are independent of the down force P_0 and the relative velocity V. This model primarily is also focused on mechanical effect, particularly the abrasion due to the abrasive-wafer and abrasive-pad contact, but it includes the chemical reaction at the wafer surface. Therefore, this model looks more comprehensive to describe the CMP process.

In SiO_2 CMP process the material removal due to chemical etch, $RR_{chemical\ etch}$, is small compared with the mechanical removal but the material removal due to chemical etch in Cu CMP process may need to be considered for more accurate results. Therefore, we ignored the chemical etch effect in the simulation of SiO_2 CMP process and the removal rate can be written as

$$RR = C_2\left(1-\Phi\left[3-C_1P_0^{1/3}\right]\right)\sqrt{P_0}V$$

Chapter 3

Optimal Control Design：Dynamic Programming

Sociological, economic, and physical pressures in all areas of modern life have generated an accelerated demand for high-level decision-making based upon limited information about the processes being controlled. In 1950s, a systematic and concerted mathematical study of such decision-making situations was initiated by Richard Bellman. This pioneering work was based upon the fundamental system-theoretic notion of feedback, i.e., that decision rules should be based upon the current (and perhaps past) states of the process under study. Bellman and his colleagues continued to develop the feedback decision-making concept under the name of "dynamic programming". The majority of problems of true practical concern were computationally intractable due to the limited state of the computing art at that time. As time goes on, a combination of rapid progress in computer technology, coupled with the development of refined computational procedures, has made it practical for solving a wide variety of problems in economics, engineering, operations research, and mathematics, itself.

3.1 Bellman's Principle of Optimality

The fundamental concept of dynamic programming originated by Bellman is called the principle of optimality. This principle may conceptually be thought as follows: Given an optimal trajectory from point A to point C, the portion of the trajectory from any intermediate point B to point C must be the optimal trajectory from B to C. In Fig. 3.1, if the path Ⅰ-Ⅱ is the optimal path from A to C, then

according to the principle of optimality path Ⅱ is the optimal path from B to C. The proof by contradiction for this case is immediate: Assume that some other path, such as Ⅱ′, is the optimum path from B to C. Then, path Ⅰ-Ⅱ′ has less cost than path Ⅰ-Ⅱ. However, this contradicts the fact that Ⅰ-Ⅱ is the optimal path from A to C, and hence Ⅱ must be the optimal path from B to C.

3.2 Dynamic Programming

Consider a quantized state $x \in X$, at stage (N-1). At this state, each of the admissible decisions $u^{(m)} \in U$ is applied.

$$X = [x^1\ x^2 \ldots x^{n-1}\ x^n]\ ,\ U = [u^1\ u^2 \ldots u^{M-1}\ u^M]$$

For each of these decisions the cost at the current stage can be determined as

$$L^{(m)} = L[x, u^{(m)}, N-1] \quad (m = 1,2,\ldots,M)$$

Next, for each of these decisions the next state at stage N is determined from the system equation,

$$x^{(m)}(N) = g[x, u^{(m)}, N-1] \quad (m = 1,2,\ldots,M)$$

The next step is to compute the minimum cost at stage N for each of the states $x^{(m)}$. However, in general a particular state $x^{(m)}$ will not lie on one of the quantized states $x \in X$ at which the optimal cost I(x, N) is defined. In fact, it may lie outside of the range of admissible states. In the latter case the decision is rejected as a candidate for the optimal decision for this state and stage. If a next state x(m) does fall within the range of allowable states, but not on a quantized value, then it is necessary to use some type of interpolation procedure to compute the minimum cost function at these points.

Assume, then that the values of the minimum cost at the states x(m) can be

expressed as a function of the values of the optimal cost at quantized states $x \in X$.

$$I[x^{(m)}, N] = P[x^{(m)}, N, I(x, N)], \text{all } x \in X$$

where $I(x, N) = L(x, N)$. If, as is often the case, no decision is made at k=N, the final stage, and hence the cost function at N depends only on the final state, x(N).

The total cost of applying decision $u^{(m)}$ at state x, stage (N-1), can then be written as

$$F_1^{(m)} = L[x, u^{(m)}, N-1] + I[x^{(m)}, N]$$

The minimization can be achieved by simply comparing the M quantities. According to the functional equation, the minimum value will be the minimum cost at state x, stage (N-1).

$$I[x, N-1] = \min_{u^{(m)} \in U} \{L[x, u^{(m)}, N-1] + I[x^{(m)}, N]\} \tag{3.1}$$

the optimal decision at this state and stage, $\hat{u}[x, N-1]$, is the control $u^{(m)}$ for which the minimum in Eq. (3.1) is actually taken on.

This procedure is repeated at each quantized state $x \in X$ at stage (N-1). When this has been done, I(x, N-1) and $\hat{u}[x, N-1]$ are known for all $x \in X$. It is now possible to compute I(x, N-2) and $\hat{u}[x, N-2]$ for all $x \in X$ based on knowledge of I(x, N-1).

The general iterative procedure continues this process. Suppose that I(x, k+1) is known for all $x \in X$. Then I(x, k) and $\hat{u}[x, k]$ are computed for all $x \in X$ from

$$I[x, k] = \min_{u^{(m)} \in U} \{L[x, u^{(m)}, k] + I[x^{(m)}, k+1]\} \tag{3.2}$$

where x(m) is determined from

$$x^{(m)} = g[x, u^{(m)}, k]$$

and where $I(x^{(m)}, k+1)$ is computed by interpolation on the known values I(x, k+1) for all $x \in X$：

$$I[x^{(m)}, k+1] = P[x^{(m)}, k+1, I(x, k+1)], \text{all } x \in X$$

The optimal decision $\hat{u}[x,k]$ is the decision for which Eq. (3.2) takes on the minimum. The iterative procedure begins by computing $\hat{u}[x,N-1]$ and I(x,N-1) from the given boundary conditions I(x, N), and it continues until $\hat{u}[x,0]$ and I(x, 0) have been computed.

The complete results of dynamic programming are shown in Fig. 3.2. At each state of stage, the optimal decision is written blow, and the minimum cost is written above. Finally, we can find the optimal sequence of decisions starting from the given x(0) and system equation. This is called the recovery procedure and these decisions are the input for our experiments. However, this is based on the system equation when we lack the measure of state. Our simulated results were done in this manner.

If we could monitor the state and stage of the system, the dynamic programming solution, $\hat{u}[x,k]$, leads to a feedback control or decision policy configuration. One method of implementing this solution is to simply store all the values of $\hat{u}[x,k]$ in memory, monitor the state and stage of the system, and look up the appropriate value of $\hat{u}[x,k]$ as required. This type of implementation is attractive because the dynamic programming calculations can be done off-line, and the only operation that needs to be done during the decision interval is retrieval of the appropriate optimal decision. The system configuration is as shown in Fig. 3.3.

3.3 Simulation Results

We used the very simple concept to get the equation for our simulation. The differential equation of the thickness being polished is equal to the removal rate and we made the removal rate to be the input. The equation is written as

$$\dot{h} = \frac{dh}{dt} = -RR = -u$$

where h is the thickness, RR the removal rate, u the input. The discretized version using a sampling period of T is

$$h(k+1) = h(k) - T \times u(k) \tag{3.3}$$

where k is the stage. We assumed that there were only 7 values of the input (include 0) because of restrictions on the Westech 372M CMP machine and the sampling period T here was fixed to 1. For each of these inputs the cost at the current stage can be determined as

$$L^{(m)} = \frac{1}{2} q h^2(k) + \frac{1}{2} r u^2(k) \quad (m = 1,2,...,7) \tag{3.4}$$

and the cost at the final stage N also was determined as

$$I(x, N) = L(x, N) = \frac{1}{2} s h_N^2 \tag{3.5}$$

where s is the weighting factor of final state, q the weighting factor of transient state, and r the weighting factor of input. Then we suppose a quantized state $h \in H$ and a admissible inputs $u^{(m)} \in U$ are applied.

$$H = [6000\ 5999\ 5998 \ldots 2\ 1\ 0]\ (jN=6001)$$

$$U = [u^{(1)}\ u^{(2)}\ u^{(3)}\ u^{(4)}\ u^{(5)}\ u^{(6)}\ u^{(7)}]\ (mN=7)$$

We could get I(h,N-1) and $\hat{u}[h, N-1]$ for all $h \in H$ by substituting Eq. 3.3, Eq. 3.4 and Eq. 3.5 into Eq. 3.2 which is presented in section 3.2.

$$I[6000, N-1], I[5999, N-1], \ldots, I[1, N-1], I[0, N-1]$$

$$\hat{u}(6000, N-1), \hat{u}(5999, N-1), \ldots, \hat{u}(1, N-1), \hat{u}(0, N-1)$$

It is now possible to compute I(h, N-2) and $\hat{u}[h, N-2]$ for all $h \in H$ based on knowledge of I(h, N-1). The iterative procedure continues until $\hat{u}[h,0]$ and I(h, 0) have been computed. The program flowchart is shown in Fig. 3.4 and the complete results of dynamic programming can be plotted like Fig. 3.2. Finally, we can find the optimal sequence of inputs starting from the given h(0) and Eq. 3.3 by means of the recovery procedure.

3.3.1 SiO_2 CMP Process

Before we start to simulate dynamic programming, we have to determine the two constants, C_1 and C_2, in the Luo and Dornfeld equation. Furthermore, we modified the power of V from 1 to 6/10 which is based on Yin's thesis [19] and the value of V means the rotational speed. Platen speed and carrier speed were all equal to the rotational speed. Two sets of experimental removal rate results are used to solve for the values of C_1 and C_2 by means of an iteration method of trial and error. The process parameters and slurry formulation used for SiO_2 CMP experiment were listed in Table 3-1 and Table 3-2, and the two set of experimental results were listed in Table 3-3. The sample and evaluation of removal rate were mentioned in chapter 4. Then, we can solve for the values of C_1 and C_2 to be 8257 and 0.322, respectively. Thus, the removal rate prediction will be

$$RR = 8257\left(1-\Phi\left[3-0.322\,P_0^{1/3}\right]\right)\sqrt{P_0}\,V^{(6/10)}.$$

Table 3-4 shows the six experimental data of removal rate when the rotational speed is fixed at 30 rpm and the down force as the variable, and when the down force is fixed at 4 psi and the rotational speed as the variable. Fig. 3.5 shows the model prediction and experimental observations of the effects of the down force and rotational speed. Because C_1 and C_2 were based on the down force, the model prediction was better on the down force model than the rotational speed model. The error bars means the non-planarization index (the deviation of the removal rates of the nine points on the wafer). The smaller the non-planarization index, the more uniform removal rate on the entire wafer and it results in more flat surface. Decreasing the down force or rotational speed will decrease the non-planarization index. We try to reduce the down force or rotational speed after SiO_2 film thickness is less than 2000 Å

to get better non-planarization index. In order to reduce the down force or rotational speed when the thickness is less than 2000 Å we choose the weighting factors of final state, transient state and input to be 10000, 1 and 100000 respectively for the case of down force, and 10000, 1 and 700 for the case of rotational speed.

(a) Change down force as the admissible input to predict removal rate

The 7 values of down force and the corresponding removal rates based on the Luo and Dornfeld equation were listed in Table 3-5 and these values were used as the admissible inputs for dynamic programming. The rotational speed was held at 30 rpm. The initial thickness h(0) was 6000 Å. Then, we started to simulate dynamic programming for optimal control of SiO_2 CMP process and the result is shown in Fig. 3.6. According to the results, the process terminated at the 363th stage and the input is 7 psi during 0st~177th stage, 4 psi during 178th~225th stage, 2.5 psi during 226th~272th stage and 2 psi during 273th~362th stage. The data was tabulated in Table 3-6 and it was the basis of our SiO_2 experiment on down force.

(b) Change rotational speed as the admissible input to predict removal rate

The down force was held at 4 psi. The initial thickness h(0) is 6000 Å, we use the model that has been calculated above to predict removal rate as we change the rotational speed. Thus, the equation removal rate prediction is repeated here

$$RR = 8257\left(1-\Phi\left[3-0.322\,P_0^{1/3}\right]\right)\sqrt{P_0}\,V^{(6/10)}.$$

The 7 values of rotational speed and the corresponding removal rates based on the Luo and Dornfeld equation were listed in Table 3-7 and these values of removal rate were used as the admissible inputs for dynamic programming. Then,

the result of dynamic programming is shown in Fig. 3.7. According to the results, the process terminated at the 334th stage and the input is 70 rpm during 0st~171th stage, 40 rpm during 172th~190th stage, 35 rpm during 191th~200th stage, 30 rpm during 201th~242th stage and 20 rpm during 243th~333th stage. The data was tabulated in Table 3-8 and it was the basis of our SiO_2 experiment on rotational speed.

(c) Change down force and rotational speed as the admissible inputs simultaneously to predict removal rate

At the beginning of the CMP process, we hoped that the removal rate was high enough to reduce the time of process and also obtained more flat surface at the end of the process. According to Dar's thesis [16], the rotational speed has a great influence on the non-uniformity. For these reason we attempted to apply both inputs. We chose the weighting factors of final state, transient state, down force and rotational speed to be 10000, 1, 50000 and 1000 respectively. The result of dynamic programming is shown in Fig. 3.8. The rotational speed is decreased first in order to get better non-planarization index when the SiO_2 film thickness is about 2000 Å and followed by the down force. The process terminated at the 237th stage. Certainly, the time was reduced compared to one admissible input. The data was tabulated in Table 3-9 and it was the basis of our SiO_2 experiment on two sets of admissible inputs.

3.3.2 Cu CMP Process

Two sets of experimental removal rate results are used to solve for the values of C_1 and C_2 as we did for the SiO_2 CMP process. Furthermore, we adopted the original

power of V to 1 based on our experimental data. Platen speed and carrier speed were all equal to the rotational speed, V. The process parameters and slurry formulation used for Cu CMP experiment were listed in Table 3-10 and Table 3-11, and the two set of experimental results were listed in Table 3-12. The simulation of Cu CMP is similar to the SiO_2 CMP and the only difference was that we had to consider the chemical etching rate in the Luo and Dornfeld equation. The chemical etching rate was obtained by experiment and the procedure was presented in chapter 4. The measured etching rate was about 14 Å/minute. It is quite small compared to the overall removal rate. The main reason was that we added a higher concentration of the citric acid. According to Ming's thesis [17], as the concentration of citric acid in the HNO_3-citric acid slurry increased, the etching rate of copper in the HNO_3-citric acid slurry was suppressed. The citric acid behaves like BTA (Benzotriazole) in preventing copper corrosion in the HNO_3-based solution. The BTA is a common Cu corrosion inhibitor since it can absorb on Cu surface to form a passivation layer. It is helpful to a Cu damascene structure because of the low etching rate at the recessed region of the Cu film. Furthermore, the removed thickness was only 6000 Å, hence we hoped that the removal rate was not too high. Therefore we omitted the chemical etching rate here. Then, we can solve for the values of C_1 and C_2 to be 30503 and 0.0113, respectively. Thus, the removal rate prediction will be

$$RR = 30503\left(1-\Phi\left[3-0.0113\,P_0^{1/3}\right]\right)\sqrt{P_0}\,V \qquad (3.6)$$

Table 3-13 shows the six experimental data of removal rate when the rotational speed is fixed at 30 rpm and the down force as the variable, and when the down force is fixed at 3.5 psi and the rotational speed as the variable. Fig. 3.9 shows the model prediction and experimental observations of the effects of the down force and rotational speed. The error bars means the non-planarization index (the deviation of

the removal rates of the nine points on the wafer). In order to decreased the down force or rotational speed in the same manner of SiO_2 when the Cu film thickness is less than 2000 Å we choose the weighting factors of final state, transient state and input to be 10000, 1 and 40000 respectively for the case of down force, and 10000, 1 and 1200 for the case of rotational speed.

(a) Change down force as the admissible input to predict removal rate

The 7 values of down force and the corresponding removal rates based on the Luo and Dornfeld equation were listed in Table 3-14 and these values were used as the admissible inputs for dynamic programming. The rotational speed was held at 30 rpm. The initial thickness h(0) was 6000 Å. Then, we started to simulate dynamic programming for optimal control of Cu CMP process and the result is shown in Fig. 3.10. According to the results, the process terminated at the 118th stage and the input is 7 psi during 0st~67th stage, 5 psi during 68th~76th stage, 4 psi during 77th~84th stage, 3.5 psi during 85th~87th stage and 3 psi during 88th~117th stage. The data was tabulated in Table 3-15 and it was the basis of our Cu experiment on down force.

(b) Change rotational speed as the admissible input to predict removal rate

The down force was held at 3.5 psi. The initial thickness h(0) is 6000 Å, we use the model that has been calculated above to predict removal rate as we change the rotational speed. Thus, the equation removal rate prediction is repeated here

$$RR = 30503\left(1-\Phi\left[3-0.0113\,P_0^{1/3}\right]\right)\sqrt{P_0}\,V .$$

The 7 values of rotational speed and the corresponding removal rates based on the Luo and Dornfeld equation were listed in Table 3-16 and these values of

removal rate were used as the admissible inputs for dynamic programming. Then, the result of dynamic programming is shown in Fig. 3.11. According to the results, the process terminated at the 85th stage and the input is 70 rpm during 0st~40th stage, 50 rpm during 41th~47th stage, 45 rpm during 48th~50th stage, 35 rpm during 51th~57th stage and 30 rpm during 58th~84th stage. The data was tabulated in Table 3-17 and it was the basis of our Cu experiment on rotational speed.

(c) Change down force and rotational speed as the admissible inputs simultaneously to predict removal rate

As we know that dishing and erosion are proportional to the pressure and rotational speed, we expected that decreasing the down force and rotational speed would improve the defects and also obtained better non-planarization index at the end of the process. Nevertheless only the blanket wafer of Cu was experimented since we lacked for pattern wafers. We chose the weighting factors of final state, transient state, down force and rotational speed to be 10000, 1, 20000 and 1200 respectively. The result of dynamic programming is shown in Fig. 3.12. The rotational speed is decreased first in order to get better non-planarization index when the Cu film thickness is about 2000 Å and followed by the down force. The process terminated at the 60th stage. Certainly, the time was reduced compared to one admissible input. The data was tabulated in Table 3-18 and it was the basis of our blanket Cu experiment on two sets of admissible inputs.

3.4 Discussion and Summary

The Westech 372M machine in National Nano Device Laboratories (NDL) has

six phases to polish a wafer and each phase can be set some important parameters, like down force, platen speed and slurry flow rate, etc.. In order to operate in co-ordination with the CMP machine we could only have 7 values of the admissible input (include 0) and the method of dynamic programming has the advantage of dealing with the constrained inputs.

The power of V in the Luo and Dornfeld equation was different between SiO_2 and Cu because of the curve fitting of experimental data. The power of V for SiO_2 and Cu were 6/10 and 1, respectively. The weighting factor of final state means the degree of final state that we want to be. The weighting factor of transient state means the speed of approaching to the final state. The last weighting factor, admissible input, means the degree of energy that we care about. In this thesis, we only want the admissible input to decrease when the thickness of SiO_2 or Cu film is less than 2000 Å. In other words, the values of these weighting factors were determined by an iteration method of trial and error.

In this chapter, three simulations of CMP operation include down force, rotational speed and both down force and rotational speed were examined. The simulated results of SiO_2 and Cu CMP process revealed that the values of admissible inputs decreased regardless of operating down force or platen speed after the thickness was less than 2000 Å. Finally, we decreased the down force and rotational speed both. We made the rotational speed decrease first in order to get better non-planarization index and then decreased the down force to reduce the removal rate. This kind of operation also reduced the duration of polishing and enhanced the throughput simultaneously.

Chapter 4

Experiment and Discussion for SiO_2 and Cu Blanket Wafer

The experiments were carried out on the IPEC 372M CMP polisher. All polishing samples were prepared on p-type, (100)-oriented, 6-inch (150 mm) diameter silicon wafers.

4.1 CMP Process for Experiment

4.1.1 Sample Preparation

The thermally grown silicon dioxide film was obtained by wet oxidation (ASM/LB45 furnace system), in which the silicon was exposed to an ambient of H_2 and O_2 at 980˚C. The sample for the SiO_2 CMP experiment was SiO_2 film grown to 9000 Å thickness by this furnace system.

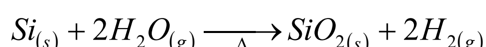

$$Si_{(s)} + 2H_2O_{(g)} \xrightarrow[\Delta]{} SiO_{2(s)} + 2H_{2(g)}$$

The sample for the blanket Cu CMP experiment is a two-layer structure of Cu/Ta with thickness of 20000/500 Å sputter deposited by ULVAC SBH-3308 RDE sputter system on the silicon wafer which is covered with a 1000 Å thick thermally grown SiO_2. The under layer of 500 Å Ta is used as an adhesion promoter for the copper deposition since copper itself does not adhere well on the thermal oxide. The structures of SiO_2 and blanket Cu CMP wafer are shown in Fig. 4.1.

4.1.2 Post CMP Cleaning

Typically post-CMP cleaning is accomplished by a combination of methods, including wet chemical cleaning, megasonic cleaning, and mechanical polyvinyl alcohol (PVA) brush scrubbing. After polishing, post-CMP cleaning returns the wafer surface to an acceptable cleanliness level. Cleaning equipment must be able to remove slurry particle, heavy surface metals, and mobile ions without leaving macroscopic, microscopic, or electrically active defects is very important in making the process useful. Removal of particles from wafer surfaces requires the application of an external force that overcomes the force of adhesion. In this work, van der Waals and electrostatic double layer interactions are considered to be the adhesion forces. CMP slurry and post chemical cleans should not introduce any chemical or particulate contamination. Thus, cleaning processes must be designed for specific materials surface. The current technology of choice for Cu and SiO_2 CMP cleaning uses one-side brush scrubbing. The experiments of this thesis use by the post-CMP cleaner of Solid State Equipment Corporation.

4.1.3 Static Etching Experiment

Fig. 4.2 shows the assembly of the experiment for static etching. Because the slurry was not refreshed, we put a magnet at the bottom of the container to produce the flow of the slurry in order to keep the reaction rate at the surface stable. It also dispersed the abrasive to suspend in the slurry and made the experiment be closed to the real circumstance of polishing. The surface of Cu faced with the magnet and kept a distance with the magnet. The slurry formulation was tabulated in Table 3.11. We set the time to immerse the wafer in the slurry to 5 minutes and assumed that the

concentration of the slurry was constant during static etching.

4.2 Evaluation of CMP Performance

4.2.1 SiO_2 and Cu Film Thickness Determination

The thicknesses of silicon dioxide thin films before and after polish process were measured by n&k analyzer thickness measurement system. The silicon dioxide film thickness was measured at 9 points, as shown in Fig. 4.3. To determine the thickness of copper film before and after CMP and static etching experiments, contact four point probe were used to measure the sheet resistance of copper film. Thickness of metal films is calculated by

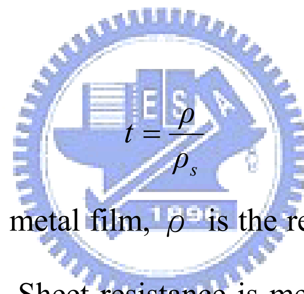

$$t = \frac{\rho}{\rho_s}$$

where t is the thickness of the metal film, ρ is the resistivity of the metal and ρ_s is the measured sheet resistance. Sheet resistance is measured at 9 points on the entire wafer in the same manner on SiO_2 and we assume the copper resistivity is unchanged after CMP and static etching experiments.

4.2.2 CMP Removal Rate and Non-Planarization Index

The CMP removal rates were monitored at 9 points along two perpendicular diameters on the entire wafer and are calculated by following formula：

$$\text{Removal Rate} = \frac{(\text{Pre-CMP Thinkness}) - (\text{Post-CMP Thinkness})}{\text{Polish Time}}$$

The chemical etch rate is defined as：

$$\text{Chemical Etch Rate} = \frac{(\text{Pre - Etch Thinkness}) - (\text{Post - Etch Thinkness})}{\text{Chemical Etch Time}}$$

The within-wafer non-planarization index is defined as：

$$\text{Non - Planarization Index} = \left(\frac{1}{n-1} \sum_{i=1}^{n} \left(x_i - \bar{x} \right)^2 \right)^{\frac{1}{2}}$$

where x is the removed thickness (Å).

4.3 SiO_2 CMP Experiment

The experiments with dynamic programming were compared with the experiments which removed the same thickness at the same duration of polishing with constant removal rate. Since the removed thickness and duration of polishing were known, we can compute the value of constant removal rate. The parameters for the constant removal rate were found through the experiment.

4.3.1 Change Down Force as the Admissible Input

The duration of polishing was 363 seconds and the removed thickness was 6000 Å. The required removal rate was 992 Å/minute. Because of the fixed rotational speed here, the required removal rate was found by changing the down force to be 4.3 psi. From the experimental results which were listed in Table 4.1 and 4.2, the constant removal rate operation mode has the better thickness removal but the dynamic programming operation mode possesses 39% better non-planarization index. The model prediction error on the lower down force caused the inaccuracy of thickness removal. It could be improved by developing more accurate model.

4.3.2 Change Rotational Speed as the Admissible Input

The duration of polishing was 334 seconds and the removed thickness was 6000 Å. The required removal rate was 1078 Å/minute. Because of the fixed down force here, the required removal rate was found by changing the rotational speed to be 40 rpm. Table 4.3 and 4.4 revealed the similar phenomenon to the part of down force. The dynamic programming operation mode possesses 26% better non-planarization index. The thickness removal was over 6000 Å for dynamic programming because the model prediction was lower than the experimental data on the higher rotational speed.

4.3.3 Change Down Force and Rotational Speed as the Admissible Inputs Simultaneously

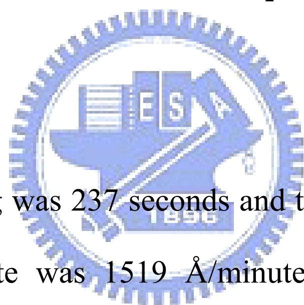

The duration of polishing was 237 seconds and the removed thickness was 6000 Å. The required removal rate was 1519 Å/minute. In order to avoid one-sided emphasis of these two inputs, we simultaneously increased the down force and rotational speed. The final value was found to be 4.7 psi and 52 rpm, respectively. The experimental results were listed in Table 4.5 and 4.6. The thickness removal had a little improvement and this might be caused by complementary model prediction. Nevertheless, the dynamic programming operation still possessed 16% better non-planarization index.

4.4 Cu CMP Experiment

The same comparison between dynamic programming and constant removal rate were discussed as we did for the SiO_2 CMP experiment. The parameters for the

constant removal rate were also found through the experiment.

4.4.1 Change Down Force as the Admissible Input

The duration of polishing was 118 seconds and the removed thickness was 6000 Å. The required removal rate was 3051 Å/minute. Because of the fixed rotational speed here, the required removal rate was found by changing the down force to be 5.1 psi. From the experimental results which were listed in Table 4.7 and 4.8, the constant removal rate has the better thickness removal but the dynamic programming possesses a little better non-planarization index. However, the difference of non-planarization index between dynamic programming and constant removal rate is very small and it may be considered within statistical error of experimental data. It also shows that the down force is not a major factor to influence the non-planarization index in Cu CMP. As shown in Fig. 3.9, we see that the non-planarization index data under 3 psi and 5 psi is within statistical error with each other. This explains why there is no degradation in non-planarization index when the down force is decreased from 5.1 psi to 3 psi, i.e. there is no degradation in non-planarization index when Cu CMP process is changed from constant removal rate operation mode to dynamic programming operation mode. The inaccuracy of removed thickness may be caused by the lower predicted value of removal rate on the smaller down force. It means that the model for Cu CMP process needs to be modified.

4.4.2 Change Rotational Speed as the Admissible Input

The duration of polishing was 85 seconds and the removed thickness was 6000 Å. The required removal rate was 4235 Å/minute. Because of the fixed down force here,

the required removal rate was found by changing the rotational speed to be 50 rpm. Table 4.9 and table 4.10 show that the dynamic programming operation mode is 24% less than the constant removal rate operation mode in non-planarization index. The error of the removed thickness may be caused by higher predicted value of removal rate at faster rotational speed and lower predicted value of removal rate at slower speed, there was not enough time to remedy lower removal rate at slower rotational speed by higher removal rate at faster rotational speed. Therefore removal thickness of dynamic programming operation mode is less than that of constant removal rate operation mode. However, it made a significant improvement of non-planarization index through dynamic programming operation of rotational speed. This shows rotational speed is a major parameter affecting the non-planarization index of Cu CMP process.

4.4.3 Change Down Force and Rotational Speed as the Admissible Inputs Simultaneously

The duration of polishing was 60 seconds and the removed thickness was 6000Å. The required constant removal rate was 6000 Å/minute. We simultaneously increased the down force and rotational speed to be 4.9 psi and 57 rpm, respectively. The experimental results were listed in Table 4.11 and 4.12. The dynamic programming operation still provides 10% improvement of non-planarization index than constant removal rate operation.

4.5 Discussion and Summary

Three cases of CMP process to use down force, rotational speed and both down

force and rotational speed as admissible inputs were examined in this chapter. In the SiO_2 CMP experiment, a summary of non-planarization index was listed in Table 4.13. Non-planarization index of three cases were all improved and the errors of the removed thickness were within 8%. The model could predict the removal rate well. It illustrated that the multi-step SiO_2 CMP was feasible to implement. Besides, it could be practiced on IPEC 372M CMP tool.

Slurry chemicals play an important role in the Cu CMP process. The formation of a non-native passivation layer by the passivating chemical (e.g. citric acid) in the slurry, the dissolution of Cu or the abraded materials by abrasives from surface layer are all determined by the chemical environment in the slurry [20]. In the Cu CMP experiment, a summary of non-planarization index was listed in Table 4.14. The result shows that the rotational speed is the main factor to influence non-planarization index. When we made the rotational speed change, non-planarization index improved 10% at least. It means that the higher the rotational speed, the faster the refresh rate of the slurry underneath the wafer and then increased the removal rate. It may also cause the worse non-uniformity of the slurry to transport on the entire wafer and exercise influence over the non-uniformity of the removal rate. For this reason, the interactions between the mechanical and chemical parameters needed to be considered anew. This also indicated that the current model was not sufficient to describe the Cu CMP. The errors of the removed thickness were above 14% and the maximum error was 25%. We brought up three ideas to eliminate the error of the removed thickness. The first way is to modify the model and make it more comprehensive and correct. The second way is to get a great number of removal rate data corresponding to every value of the admissible input by experiment and then get a better regression model. The last way is to assemble a sensor to measure the thickness at every stage and we could implement the dynamic programming solution which was illustrated in chapter 3. Mirra, the

CMP tool provided by Applied Materials, had the technology of In Situ Rate Monitor (ISRM). ISRM technology detects film thickness changes during polishing by laser interferometry system that allows the user to precisely defined material removal.

Chapter 5

Pattern Copper Wafer

5.1 Introduction

In pattern Cu CMP, the copper is removed following a three-step procedure as show in Fig. 5.1. In the planarization step, the overburden Cu is removed and the objective is to reduce the step height (difference between high and low features). This is followed by the planarization/overpolishing step where overburden metal and some barrier are removed. The wafer is further overpolished to remove residual metal. By intuition, these two defects of dishing and erosion should become more serious as the overpolishing time of the Cu CMP process increased. Therefore, the non-planarization index of Cu CMP must be reduced to minimum to minimize the dishing and erosion of the polished wafer. The pattern dependence of the metal dishing and oxide erosion of Cu damascene structure had been reported by some paper [21][22][23][29]. In this study, we focus on the step height reduction, i.e. planarization efficiency.

The model proposed by Chen and Lee [24][25] provides an excellent description of step height reduction when the wafer and pad contact each other at any point on the interface. The major assumptions in this model are：1) the pressure difference between the high area and the low area is proportional to the step height, and 2) higher area will experience higher pressure. The model proposed by Fu and Chandra [26] incorporated the effects of feature scale wafer geometries (e.g., line-width, pitch and pattern density). However, the model was also assumed that the wafer and pad were in contact at any point of the interface. It means that the pad contact with both high and

low areas. It may not be correct when the initial step height is large than pad bending, especially for a hard pad. The Rodel IC1400 pad is composed of the IC1000 stacked on top of the Suba IV and it belongs to a hard pad. Typically, the IC1400 pad is used in pattern wafer experiments. The advantage of the hard pad for the planarization step is that it has small deformations because of its limited compressibility and will ideally touch only the high area to provide good planarity. Generally, if a soft pad, e.g., Rodel Politex Regular E.^{TM} pad, was used to polish the pattern wafer, it will lead to the step topography still exist. Because the deformation and compressibility under the down force of the soft pad is serious, the high and low areas were polished simultaneously. As a consequence, the step topography still would exist and the goal of planarization was not reached.

5.2 Model Development

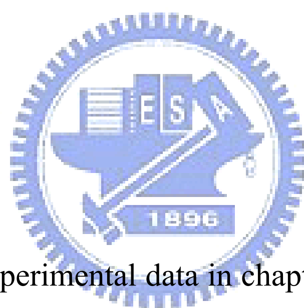

1896

Since we analyzed the experimental data in chapter 4, we found that the Luo and Dornfeld equation was unable to fit very well in copper CMP process. Therefore, the power function was used.

$$RR = KP^{a}V^{b}$$

The values of the exponents a and b were determined by the method of regression and were 0.38 and 0.85, respectively. As shown in Fig. 5.3, the experimental results can be fitted more accurately as compared with the Luo and Dornfeld equation. The model SSE values for the power function model and the Luo and Dornfeld model were 143270 and 388260, respectively. Then, the power function model is used to predict the Cu removal rate.

To physically explain the development of step height reduction during Cu CMP process, the following assumptions were made：

1. Power function is valid for all polish conditions.
2. Force redistribution due to pad bending is proportional to step height.
3. Critical pressure is determined by the pressure of the low area.
4. The pattern effect is negligible to the rotational speed.

Due to the pad bending, there exists force redistribution. This causes the contact force to drop in the low area. To maintain overall force balance due to the applied down pressure, P_0, there is a corresponding rise in the force in the high area. The total area in the high region with unit thickness (length into the page) is (b-a)·1 and the low area is a·1. The modified pressure equations including pad bending effects are

$$P_h (b-a) \cdot 1 + P_L a \cdot 1 = P_0 b \cdot 1 \tag{5.1}$$

$$P_h - P_L = \alpha S \tag{5.2}$$

Solving Eq. 5.1 and Eq. 5.2, we have

$$P_h = P_0 + \alpha \left(\frac{a}{b}\right) S \tag{5.3}$$

$$P_L = P_0 - \alpha \left(\frac{b-a}{b}\right) S \tag{5.4}$$

where P_h and P_L are the pressures on the high and low areas, a and b are the line-width and pitch and α is the pad bending stiffness parameter. Fig 5.2 shows the schematic picture.

The critical pressure is

$$P_L = P_0 - \alpha \left(\frac{b-a}{b}\right) S \tag{5.5}$$

For $P_L<0$, only the high area is polished and we have

$$P_h (b-a) = P_0 b$$

$$P_h = \left(\frac{b}{b-a}\right) P_0 \tag{5.6}$$

$$P_L=0 \tag{5.7}$$

and from Eq. 5.6 and Eq. 5.7 we can formulate the model for the pressure of low area

smaller than zero or equal zero.

$$\frac{dH}{dt} = -\left\{K\left(\left(\frac{b}{b-a}\right)P_0\right)^{0.38} V^{0.85}\right\} \tag{5.8}$$

$$\frac{dL}{dt} = 0 \tag{5.9}$$

$$\frac{dS}{dt} = -\left\{K\left(\left(\frac{b}{b-a}\right)P_0\right)^{0.38} V^{0.85}\right\} \tag{5.10}$$

where H is the height of the high area, L is the height of the low area and S is the step height. The model switch to the following set from Eq. 5.3 and Eq. 5.4 when the critical pressure is larger than zero

$$\frac{dH}{dt} = -\left\{K\,(P_0 + \alpha\,(\frac{a}{b})S)^{0.38} V^{0.85}\right\} \tag{5.11}$$

$$\frac{dL}{dt} = -\left\{K\,(P_0 - \alpha\,(\frac{b-a}{b})S)^{0.38} V^{0.85}\right\} \tag{5.12}$$

$$\frac{dS}{dt} = -\{\,K\,(P_0 + \alpha\,(\frac{a}{b})S)^{0.38} V^{0.85} - K\,(P_0 - \alpha\,(\frac{b-a}{b})S)^{0.38} V^{0.85}\} \tag{5.13}$$

In the model development, Eq. 5.2 represented the additional force imparted on the high area and corresponding decrease in the force imparted on the low area due to bending of the pad. α is the bending stiffness parameter in the model. It is not known a priori in the model. For the later comparison of the model prediction to the experimental observation, α is used as a fitting parameter.

5.3 Simulation

We used the experimental data from Stavreva etc. [22] and in the experiments, Cu CMP is carried out by the perforated Rodel IC 1000/Suba IV stacked pad. One of the experimental data points was chosen to obtain the α value corresponding to the experimental conditions. Model prediction was compared with experimental data in

Fig. 5.4. The relevant experimental parameters were given below:

(1) down force P_0 = 3.2 psi

(2) rotational speed V = 51 rpm

(3) initial step height = 6000 Å

(4) line-width = 2 μm

(5) pitch = 4 μm

(6) $\alpha = 1.393 \times 10^{11}$

Once appropriate models were constructed (e.g. Eq. 5.8-5.13) and the model parameter α were obtained, we were able to analysis the step height for different operation values through the simulation. The polish time and initial step height were set to be 1 minute and 4000 Å, respectively.

The polishing action progresses in both high and low areas. The most efficient method in planarization is to remove the high area only, but this is difficult in a real polishing process. The planarization efficiency which indicates the step height reduction in the CMP process, can be defined as

$$\text{Planarization Efficiency} = 1 - \frac{\Delta \text{Low Area}}{\Delta \text{High Area}}$$

where △low area is the removed thickness of low area and △high area is the removed thickness of high area.

Fig. 5.5 shows the planarization efficiency can be increased under a lower down force. When the down force is larger, there is the more possibility of polishing the low area and decreases the planarization efficiency. This means that the step height reduction can be improved by polishing at the lower pressure. The method of the dynamic programming could implement this kind of operation. The down force is decreased as polishing continues to the end and planarization efficiency is increased according to the simulation result. More flat surface of wafer is obtained. Moreover,

non-planarization index can be improved by decreasing the rotational speed as discussed in chapter 4. Consequently, the planarity could be improved by decreasing the down force and rotational speed simultaneously.

5.4 Discussion and Summary

In this chapter we constructed the model for describing the step height reduction and obtained the effect of down force on the planarization efficiency. Through the result of simulation we could find that the lower down force can increase the planarization efficiency. The method of dynamic programming could decreases the down force and rotational speed simultaneously and produces the higher planarization efficiency and the less non-planarization index at the same time.

Step height, dishing and erosion are three parameters that are typically used to characterize CMP of pattern wafers. If we could minimize the step height at the end of the planarization step, the high removal selectivity of the barrier layer between Cu and SiO_2 could be applied in the planarization/overpolishing step. Dishing and erosion mainly occurs during the overpolished step which is often necessary to assure complete removal of copper and barrier residues across the entire wafer [30][31]. Since the non-planarization index has been improved in the planarization step, the duration of the overpolished step could be reduced and then the goal of planarization is achieved by the three-step procedure.

Chapter 6

Conclusion and Future Work

In this study, the subject was emphasized on the mechanical parameters of the CMP process. The down force and rotational speed were taken as the control parameter. We applied the control method of dynamic programming to the CMP process and experimented with blanket SiO_2 and Cu wafers. The impacts of dynamic operation and constant removal operation on the non-planarization index after CMP process were discussed. The non-planarization index could be improved by dynamic programming operation and the rotational speed seems to be a major factor to influence the non-planarization index. The effect of the down force on the pattern wafer was focused on the planarization efficiency and the simulation result was presented. According to the simulation, the lower down force improves the planarization efficiency. Therefore, the dynamic programming operation is a feasible operational strategy for the CMP process to improve non-planarization index and planarization efficiency.

For future works, the following directions can be considered: (1) The CMP model proposed by Luo and Dornfeld should be reconstructed or modified in the copper CMP process. (2) The number of experimental wafers should be increased to provide more valid data. (3) In order to apply the dynamic programming operation on the pattern wafer, the performance index has to be reconsidered to improve step height. (4) The experiment can be carried out to varify the simulation result.

Table 2-1 The Parameters of CMP Process

- Slurry Chemicals
  - pH
  - Buffering Agents
  - Oxidizers
  - Complexing Agents
  - Concentration
  - Dielectric Constant
  - Slurry Abrasive
  - Type
  - Size
  - Concentration
  - Isoelectric point (pH)
  - zeta potential
  - Stability of the Suspension
- Slurry Flow Rate
  - Transport Under the Wafer
- Temperature
- Pressure
- Velocity
  - Pad
  - Wafer
- Frictional Forces/Lubrication
- Pattern Geometries
  - Feature Size
  - Pattern Density
- Pad
  - Fiber Structure, Height
  - Pore Size
  - Compressibility
  - Elastic and Shear Modulus
  - Hardness
  - Thickness
  - Embossing or Perforations
  - Conditioning
  - Aging Effects
  - Chemical Durability/Reactivity
- Wafer Curvature
- Wafer Mounting
- Film Stack
- Film Stress
- Film Hardness
  - Creep
  - Work Hardening, Fatigue
- Film Microstructure
- Wafer Cleaning Sequence
- Wafer Size

Table 3-1 Process Parameters of SiO_2 CMP Experiment

Fixed Parameter	Value
Down Force	2, 3, 4, 7 psi
Back Pressure	1 psi
Carrier Speed	20, 30, 70 rpm
Platen Speed	20, 30, 70 rpm
Polish Time	1 minute
Slurry Flow Rate	150 ml/minute
Pre-wet Pad Speed	28 rpm
Pre-wet Duration	10 second
Pre-wet Flow Rate	300 ml/minute
Pad	Rodel IC1400

Pad Conditioning (after polishing)	Value
Condition Pressure	0.3 psi
Platen Speed	30 rpm
Clean Speed	4 rpm
Slurry Flow Rate	150 ml/minute
Duration	30 second
Frequency	1 wafer

Table 3-2 Slurry Formulation of SiO_2 CMP

	Species	Concentration
Commercial Slurry	Cabot SS-25	1
Dilution	DI water	1

Table 3-3 The Experimental Results of SiO_2 CMP to Determine C_1 and C_2

	Set 1	Set 2
Down Force (psi)	3	7
Removal Rate (Å/minute)	618	1440

Table 3-4 The Experiment Data of SiO_2 CMP

Rotational Speed fixed at 30 rpm	Down Force (psi)	2	3	7
	Removal Rate (Å/minute)	387	618	1440
Down Force fixed at 4 psi	Rotational Speed (rpm)	20	30	70
	Removal Rate (Å/minute)	649	883	1431

Table 3-5 The Values of Admissible Inputs by Corresponding Down Force

No.	1	2	3	4	5	6	7
Down Force (psi)	2	2.5	3	3.5	4	7	0
Removal Rate (Å/minute)	426	521	618	715	814	1440	0

Table 3-6 The Result of Dynamic Programming of SiO_2 CMP with Down Force

Phase	1	2	3	4
Duration (second)	178	48	47	90
Down Force (psi)	7	4	2.5	2

Table 3-7 The Values of Admissible Inputs by Corresponding Rotational Speed

No.	1	2	3	4	5	6	7
Rotational Speed (rpm)	20	25	30	35	40	70	0
Removal Rate (Å/minute)	639	730	814	893	968	1354	0

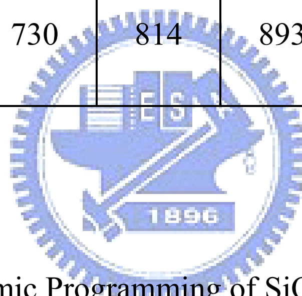

Table 3-8 The Result of Dynamic Programming of SiO_2 CMP with Rotational Speed

Phase	1	2	3	4	5
Duration (second)	172	19	10	42	91
Rotational Speed (rpm)	70	40	35	30	25

Table 3-9 The Result of Dynamic Programming of SiO_2 CMP with Two Inputs

Phase	1	2	3	4	5
Duration (second)	96	49	33	17	42
Down Force (psi)	7	7	4	2.5	2
Rotational Speed (rpm)	70	40	20	20	20

Table 3-10 Process Parameters of Cu CMP Experiment

Fixed Parameter	Value
Back Pressure	1 psi
Down Force	3, 3.5, 5, 7 psi
Carrier Speed	30, 50, 70 rpm
Platen Speed	30, 50, 70 rpm
Polish Time	1 minute
Slurry Flow Rate	150 ml/minute
Pre-wet Pad Speed	28 rpm
Pre-wet Duration	10 second
Pre-wet Flow Rate	300 ml/minute
Pad	Rodel IC1400
Pad condition	No (Manual Brushing)

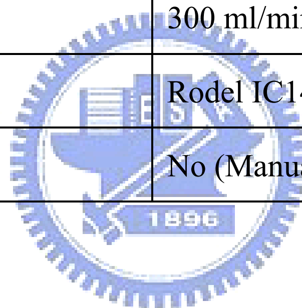
1896

Table 3-11 Slurry Formulation of Cu CMP

	Species	Concentration
Abrasive	Al_2O_3 (EXTEC 0.1μm)	2 wt %
Oxidizer	HNO_3	2 vol %
Complex Agent	Citric Acid	0.01 M
Dilution	DI water	Remaining Balance of Slurry

Table 3-12 The Experimental Results of Cu CMP to Determine C_1 and C_2

	Set 1	Set 2
Down Force (psi)	5	7
Removal Rate (Å/minute)	2942	3508

Table 3-13 The Experiment Data of Cu CMP

Rotational Speed fixed at 30 rpm	Down Force (psi)	3	5	7
	Removal Rate (Å/minute)	2522	2942	3508
Down Force fixed at 3.5 psi	Rotational Speed (rpm)	30	50	70
	Removal Rate (Å/minute)	2595	4396	5266

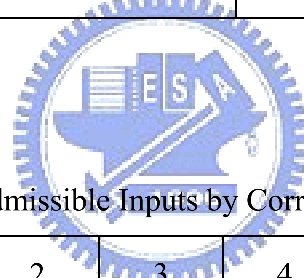

Table 3-14 The Values of Admissible Inputs by Corresponding Down Force

No.	1	2	3	4	5	6	7
Down Force (psi)	3	3.5	4	4.5	5	7	0
Removal Rate (Å/minute)	2257	2445	2620	2786	2942	3508	0

Table 3-15 The Result of Dynamic Programming of Cu CMP with Down Force

Phase	1	2	3	4	5
Duration (second)	68	9	8	3	30
Down Force (psi)	7	5	4	3.5	3

Table 3-16　The Values of Admissible Inputs by Corresponding Rotational Speed

No.	1	2	3	4	5	6	7
Rotational Speed (rpm)	30	35	40	45	50	70	0
Removal Rate (Å/minute)	2445	2852	3259	3667	4074	5704	0

Table 3-17　The Result of Dynamic Programming of Cu CMP with Rotational Speed

Phase	1	2	3	4	5
Duration (second)	41	7	3	7	27
Rotational Speed (rpm)	70	50	45	35	30

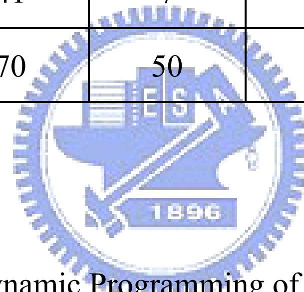

Table 3-18　The Result of Dynamic Programming of Cu CMP with Two Inputs

Phase	1	2	3	4	5	6
Duration (second)	31	3	4	4	7	11
Down Force (psi)	7	7	7	7	5	4
Rotational Speed (rpm)	70	50	45	40	30	30

Table 4.1 SiO_2 Blanket Wafer Experimental Result by Down Force with Dynamic Programming

Point NO.	1	2	3	4	5	6	7	8	9
Pre-Polish Thickness (Å)	9009	9004	9016	9003	8997	9031	9059	9009	8998
After-Polish Thickness (Å)	2999	3918	3361	3841	3805	3979	3204	3724	2807
Removed Thickness (Å)	6010	5086	5655	5162	5192	5052	5855	5285	6191
Average Removed Thickness (Å)			5499		Non-Planarization Index			435	

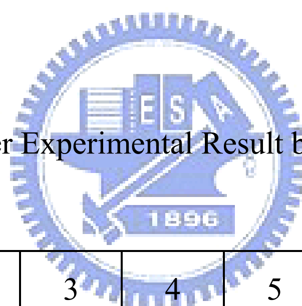

Table 4.2 SiO_2 Blanket Wafer Experimental Result by Down Force with Constant Removal Rate

Point NO.	1	2	3	4	5	6	7	8	9
Pre-Polish Thickness (Å)	9005	9004	9013	9003	8997	9026	9052	8999	8989
After-Polish Thickness (Å)	2190	3828	3714	2903	2449	3367	2112	3765	3673
Removed Thickness (Å)	6815	5176	5299	6100	6548	5659	6940	5234	5316
Average Removed Thickness (Å)			5899		Non-Planarization Index			717	

Table 4.3 SiO_2 Blanket Wafer Experimental Result by Rotational Speed with Dynamic Programming

Point NO.	1	2	3	4	5	6	7	8	9
Pre-Polish Thickness (Å)	9008	9005	9017	9007	8999	9032	9058	9006	8996
After-Polish Thickness (Å)	2122	2820	2584	3230	2185	3347	2916	3553	3351
Removed Thickness (Å)	6886	6185	6433	5777	6814	5685	6142	5453	5645
Average Removed Thickness (Å)	6113				Non-Planarization Index	518			

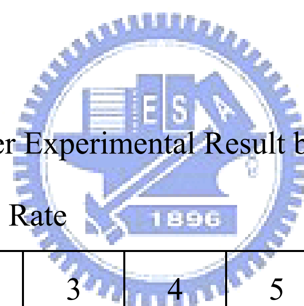

Table 4.4 SiO_2 Blanket Wafer Experimental Result by Rotational Speed with Constant Removal Rate

Point NO.	1	2	3	4	5	6	7	8	9
Pre-Polish Thickness (Å)	9004	8995	9002	8997	8988	9025	9049	9001	8986
After-Polish Thickness (Å)	1867	3747	3915	3530	3484	2936	2449	3374	2519
Removed Thickness (Å)	7137	5248	5087	5467	5504	6089	6600	5627	6467
Average Removed Thickness (Å)	5914				Non-Planarization Index	697			

Table 4.5 SiO_2 Blanket Wafer Experimental Result by Two Admissible Inputs with Dynamic Programming

Point NO.	1	2	3	4	5	6	7	8	9
Pre-Polish Thickness (Å)	9013	9012	9023	9013	9003	9033	9057	9009	8997
After-Polish Thickness (Å)	2400	3673	2569	3525	3231	3789	2961	3315	2820
Removed Thickness (Å)	6613	5339	6454	5488	5772	5244	6096	5694	6177
Average Removed Thickness (Å)			5875		Non-Planarization Index			487	

Table 4.6 SiO_2 Blanket Wafer Experimental Result by Two Admissible Inputs with Constant Removal Rate

Point NO.	1	2	3	4	5	6	7	8	9
Pre-Polish Thickness (Å)	8995	8992	9000	8995	8988	9020	9044	9000	8988
After-Polish Thickness (Å)	1838	3355	3454	3008	2602	3395	2691	3676	3386
Removed Thickness (Å)	7157	5637	5546	5987	6386	5625	6353	5324	5602
Average Removed Thickness (Å)			5957		Non-Planarization Index			580	

Table 4.7 Cu Blanket Wafer Experimental Result by Down Force with Dynamic Programming

Point NO.	1	2	3	4	5	6	7	8	9
Pre-Polish Thickness (Å)	20000	20000	20000	20000	20000	20000	20000	20000	20000
After-Polish Thickness (Å)	13576	13702	13346	13037	12898	12313	11935	11954	9822
Removed Thickness (Å)	6424	6298	6654	6963	7102	7687	8065	8046	10178
Average Removed Thickness (Å)	7491				Non-Planarization Index	1204			

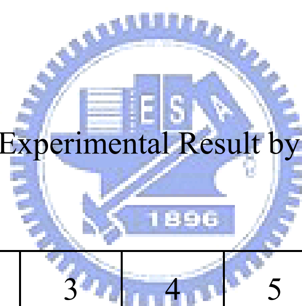

Table 4.8 Cu Blanket Wafer Experimental Result by Down Force with Constant Removal Rate

Point NO.	1	2	3	4	5	6	7	8	9
Pre-Polish Thickness (Å)	20000	20000	20000	20000	20000	20000	20000	20000	20000
After-Polish Thickness (Å)	14173	13673	14736	14616	13902	11235	12015	12512	12653
Removed Thickness (Å)	5827	6327	5264	5384	6098	8765	7985	7488	7347
Average Removed Thickness (Å)	6721				Non-Planarization Index	1225			

Table 4.9 Cu Blanket Wafer Experimental Result by Rotational Speed with Dynamic Programming

Point NO.	1	2	3	4	5	6	7	8	9
Pre-Polish Thickness (Å)	20000	20000	20000	20000	20000	20000	20000	20000	20000
After-Polish Thickness (Å)	14327	15130	15423	15047	15240	14298	13787	13941	14151
Removed Thickness (Å)	5673	4870	4577	4953	4760	5702	6213	6059	5849
Average Removed Thickness (Å)			5406		Non-Planarization Index			615	

Table 4.10 Cu Blanket Wafer Experimental Result by Rotational Speed with Constant Removal Rate

Point NO.	1	2	3	4	5	6	7	8	9
Pre-Polish Thickness (Å)	20000	20000	20000	20000	20000	20000	20000	20000	20000
After-Polish Thickness (Å)	14501	14475	14993	14216	14369	13620	13821	14298	12179
Removed Thickness (Å)	5499	5525	5007	5784	5631	6380	6179	5702	7821
Average Removed Thickness (Å)			5948		Non-Planarization Index			806	

Table 4.11 Cu Blanket Wafer Experimental Result by Two Admissible Inputs with Dynamic Programming

Point NO.	1	2	3	4	5	6	7	8	9
Pre-Polish Thickness (Å)	20000	20000	20000	20000	20000	20000	20000	20000	20000
After-Polish Thickness (Å)	13417	14200	14352	13866	13975	11720	12423	13049	11677
Removed Thickness (Å)	6583	5800	5648	6134	6025	8280	7577	6951	8323
Average Removed Thickness (Å)			6814		Non-Planarization Index			1034	

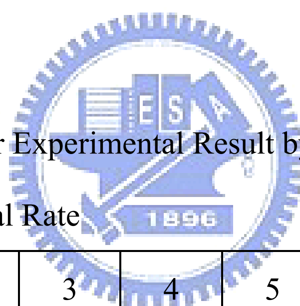
E S A 1896

Table 4.12 Cu Blanket Wafer Experimental Result by Two Admissible Inputs with Constant Removal Rate

Point NO.	1	2	3	4	5	6	7	8	9
Pre-Polish Thickness (Å)	20000	20000	20000	20000	20000	20000	20000	20000	20000
After-Polish Thickness (Å)	14538	15339	15691	14444	15212	12953	13293	14264	12319
Removed Thickness (Å)	5462	4661	4309	5556	4788	7047	6707	5736	7681
Average Removed Thickness (Å)			5772		Non-Planarization Index			1153	

Table 4.13 Comparison of Non-Planarization Index (SiO_2 Blanket Wafer)

	Down Force	Rotational Speed	Down Force + Rotational Speed
Conventional	717	697	580
Dynamic Programming	435	518	487
Improvement by Dynamic Programming	39 %	26 %	16 %

Table 4.14 Comparison of Non-Planarization Index (Cu Blanket Wafer)

	Down Force	Rotational Speed	Down Force + Rotational Speed
Conventional	1225	806	1153
Dynamic Programming	1204	615	1034
Improvement by Dynamic Programming	2 %	24 %	10 %

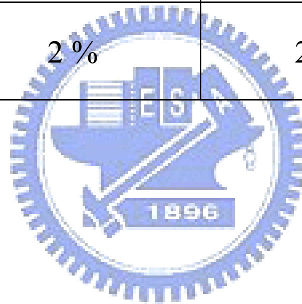

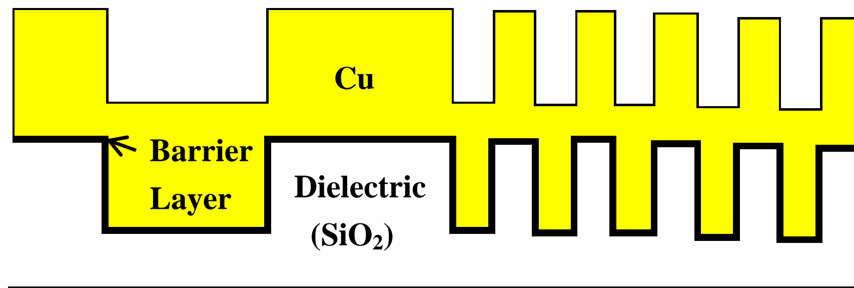

(a)

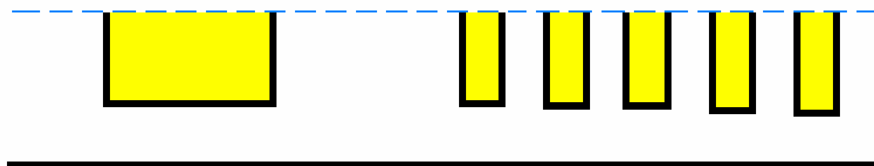

(b)

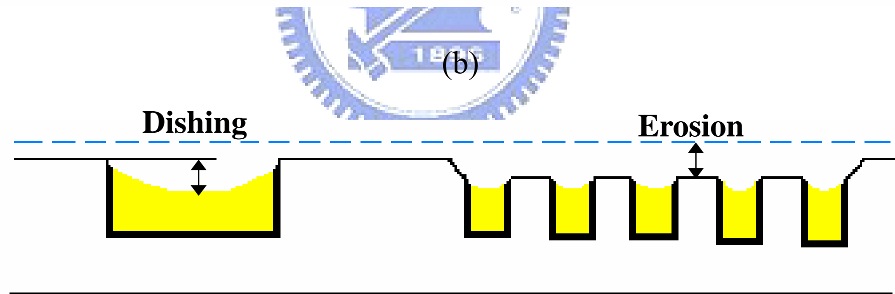

(c)

Figure 1.1 Schematics of a Single Layer Cu Interconnect： (a) Before Polishing (b) Ideal Case After Polishing and (c) Real Case After Polishing

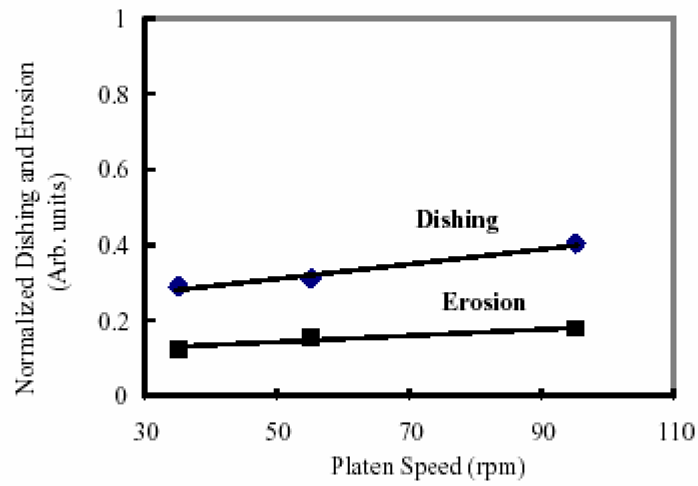

Figure 1.2 (a) Dependence of Copper Dishing and Oxide Erosion on Platen Speed. Wafer Pressure was Kept Constant. [10]

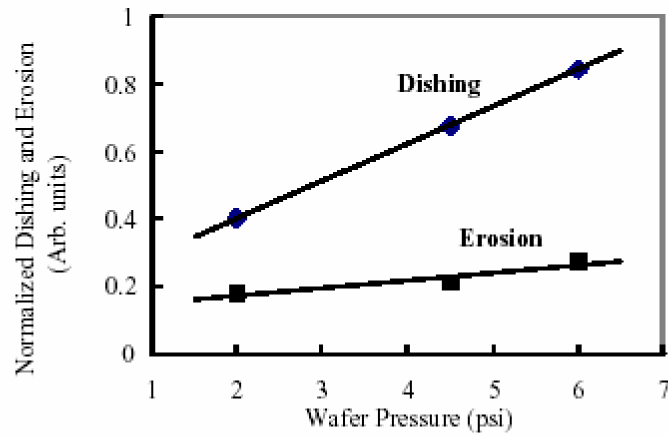

Figure 1.2 (b) Dependence of Copper Dishing and Oxide Erosion on Wafer Pressure. Platen Speed was Held Constant. [10]

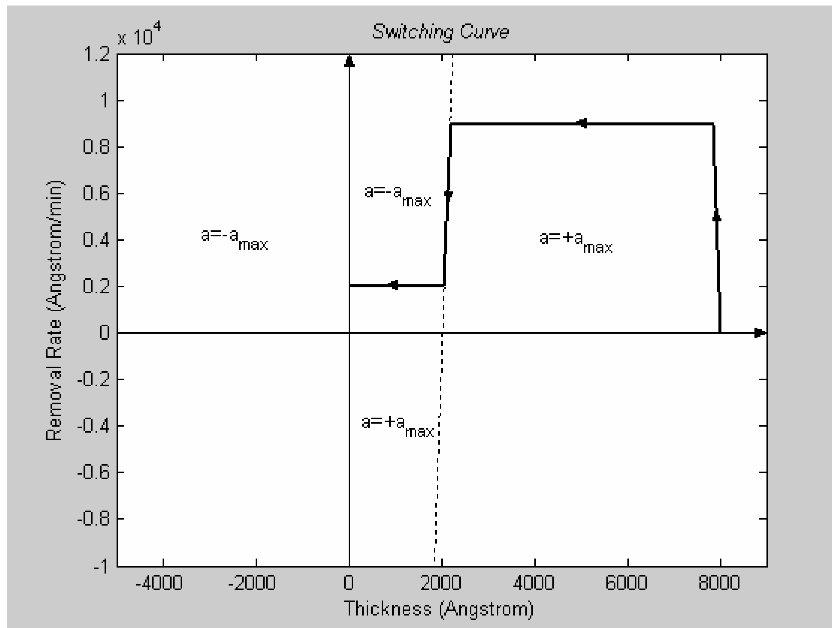

(a)

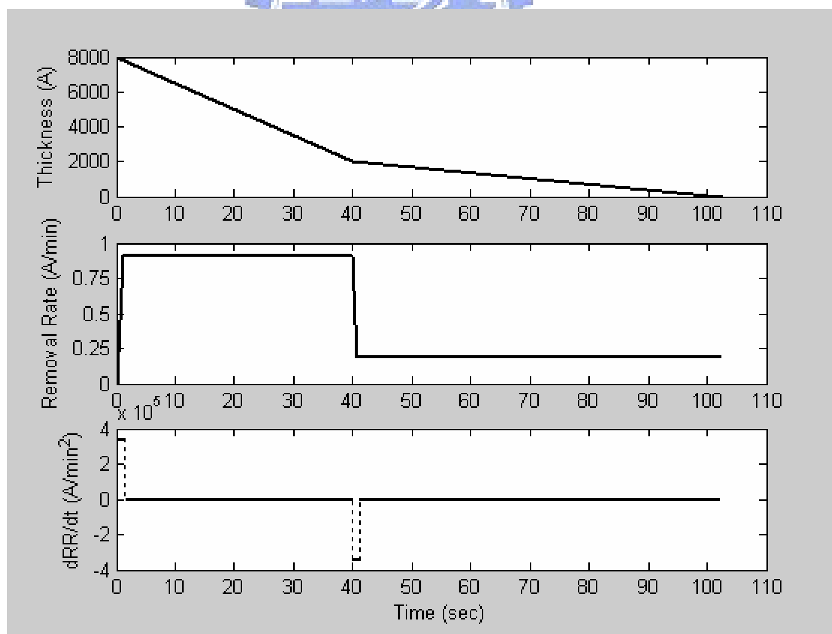

(b)

Figure 1.3 Trajectory for RR_{max}=9000 Å/min, u_{max}=360000 Å/min^2, H_{small}=2000 Å, and RR_{small}=2000 Å/min [9]

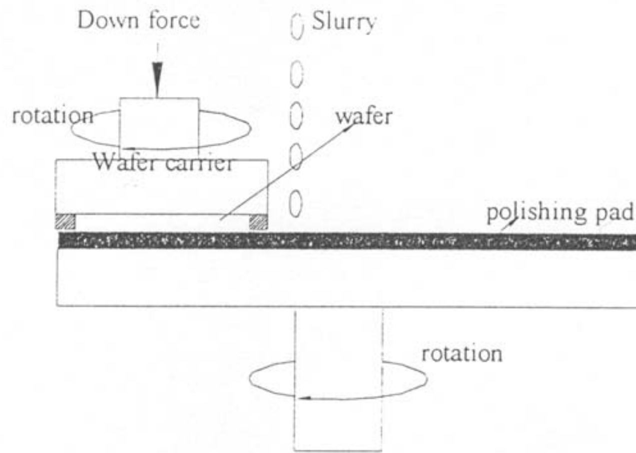

Figure 2.1 The Mimic Schematic of CMP

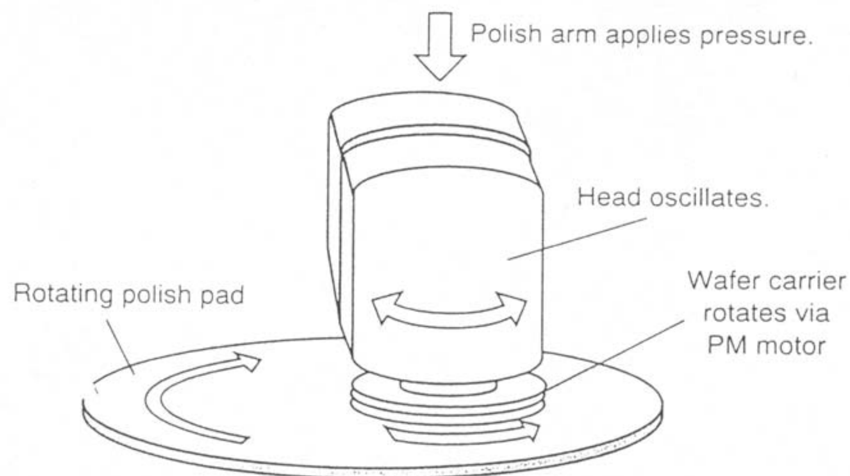

Figure 2.2 CMP Motion

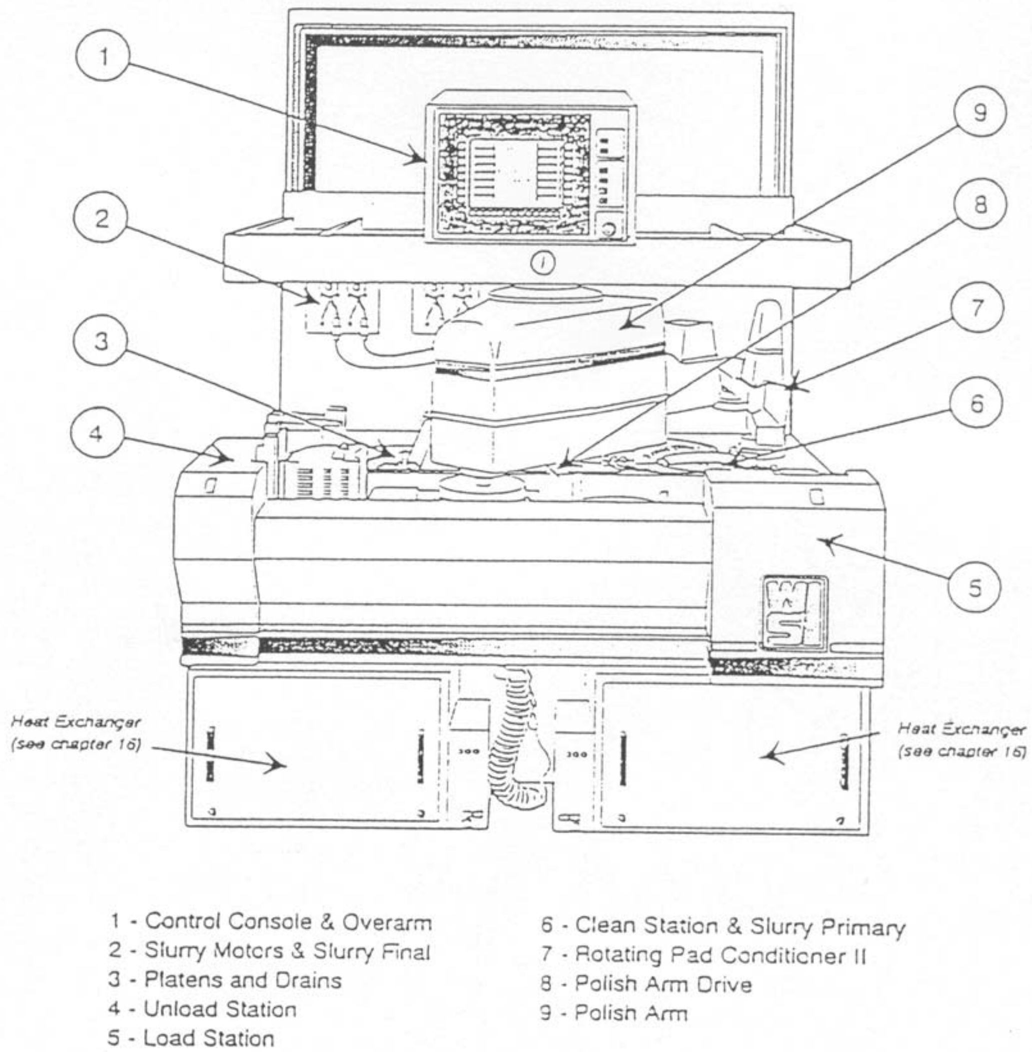

Figure 2.3 The Perspective Front-View of CMP System- Westech 372M Machine

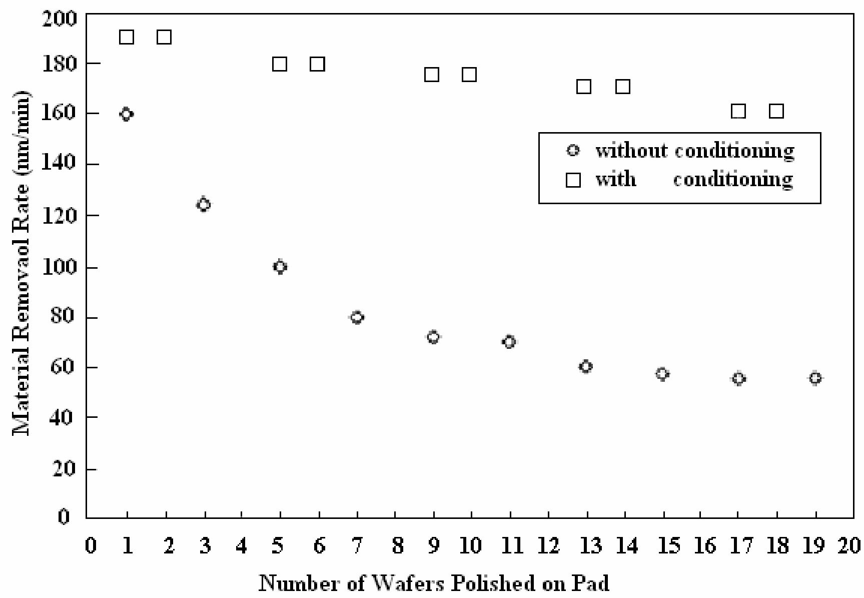

Figure 2.4 The Removal Rate Curves for Pad with Conditioning and without Conditioning [8]

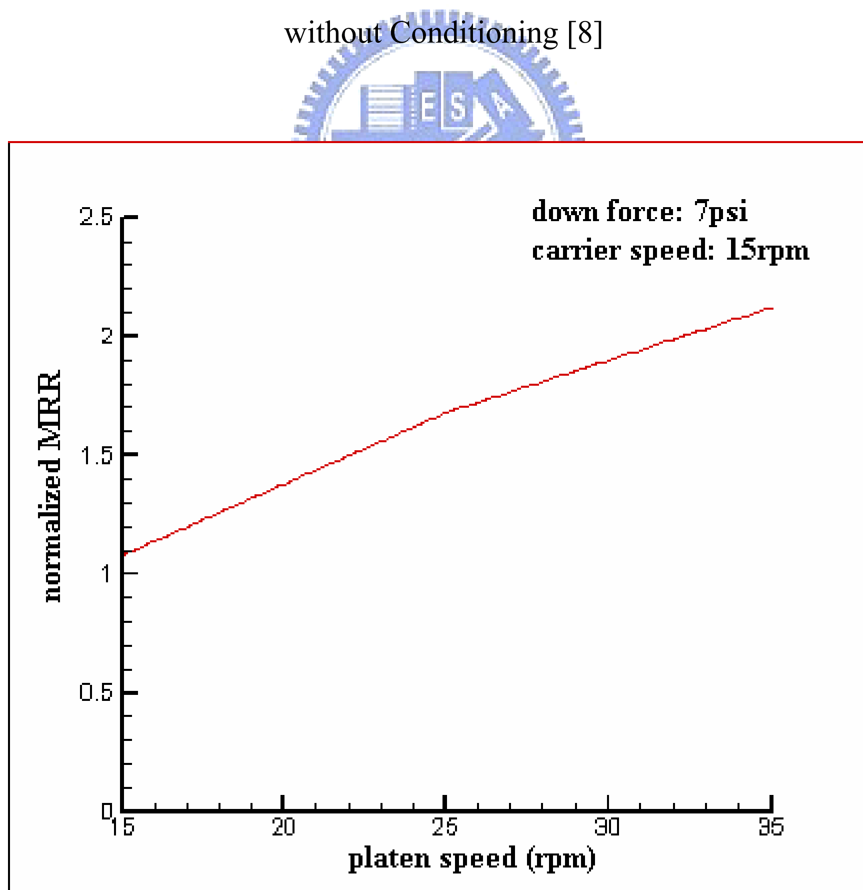

Figure 2.5 The Removal Rate Curve for Platen Speed [16]

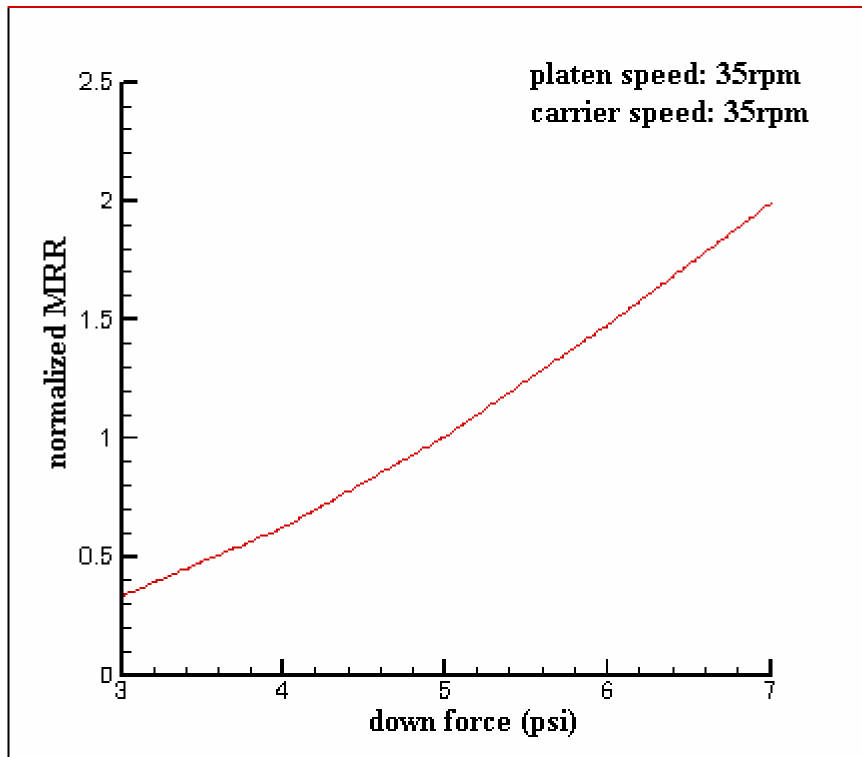

Figure 2.6 The Removal Rate Curve for Down Force [16]

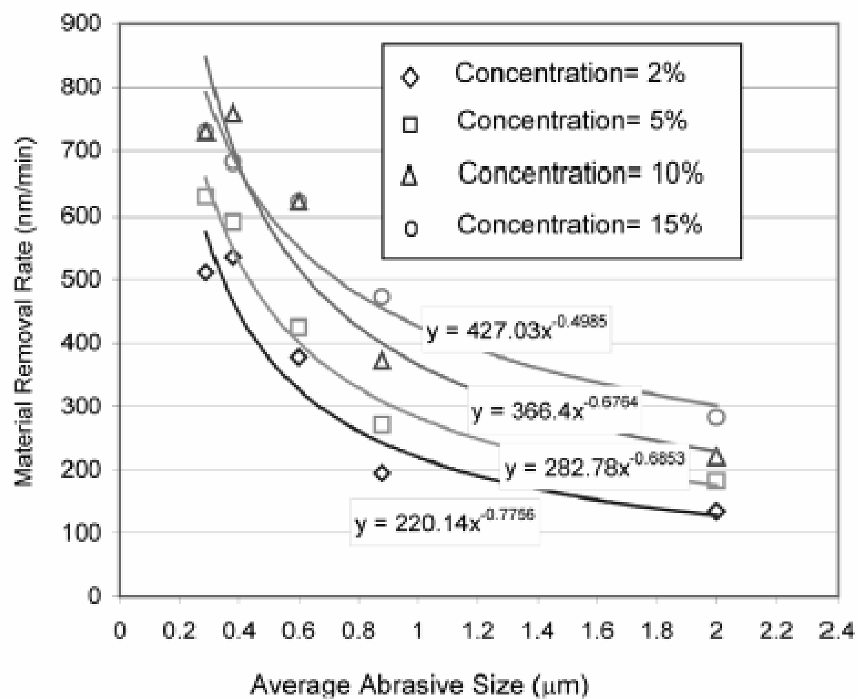

Figure 2.7 MRR as a Function of Abrasive Size Distribution and Abrasive Weight Concentration [11]

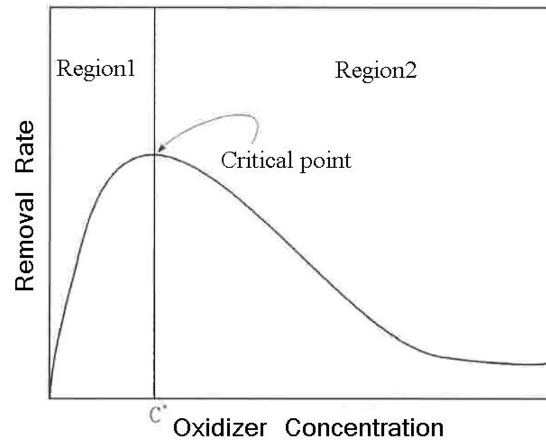

Figure 2.8 Effects of Oxidizer Concentration on Removal Rate [12]

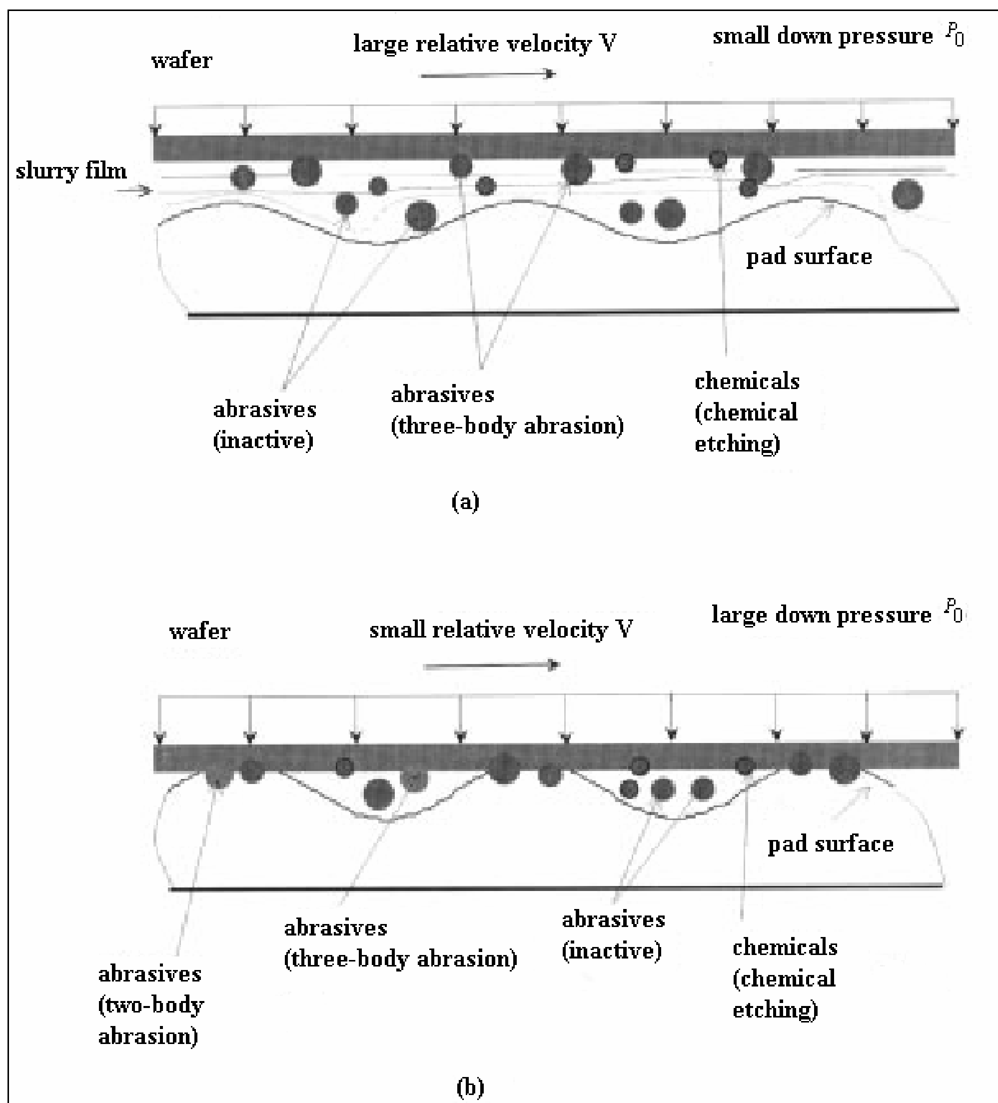

Figure 2.9 Two Contact Modes of CMP：(a) Hydro-Dynamic Contact Mode and

(b) Solid-Solid Contact Mode [8]

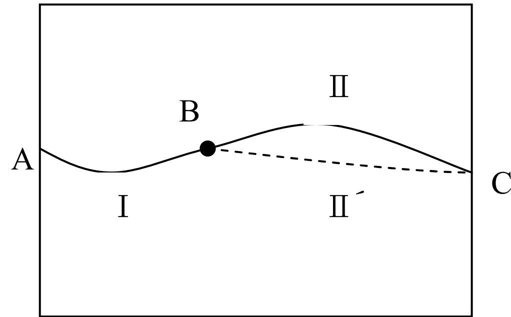

Figure 3.1 Illustration of the Principle of Optimality

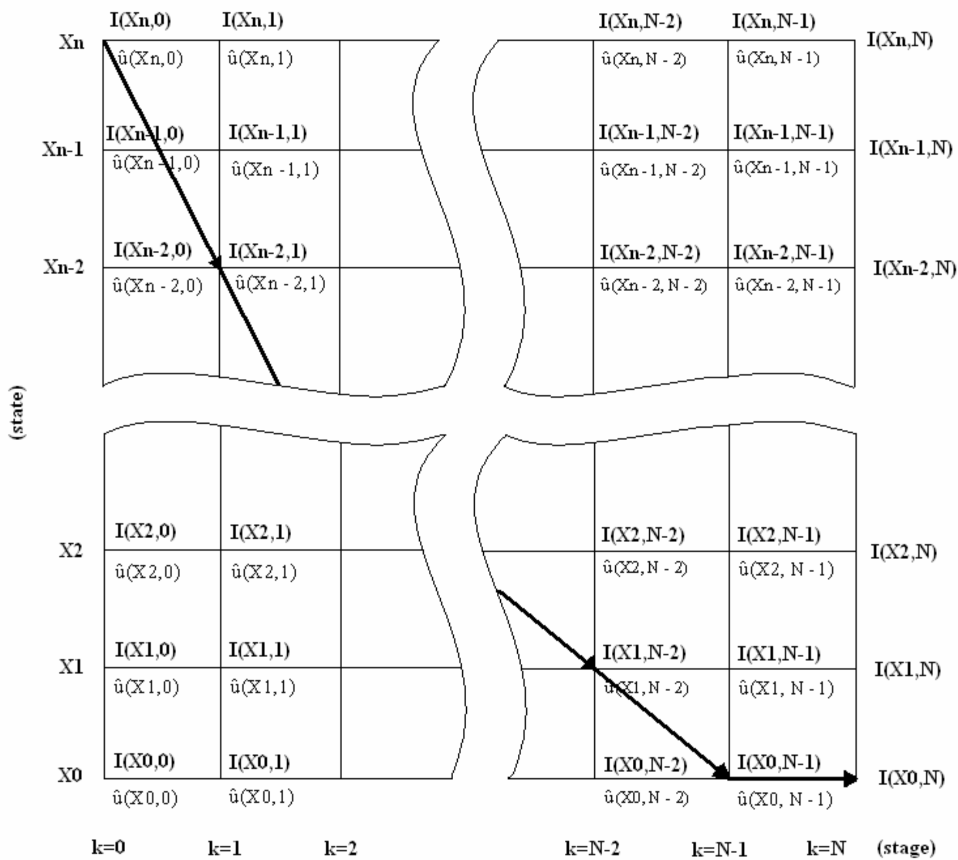

Figure 3.2 Complete Result of Dynamic Programming and Recovery of the Optimal Trajectory from Initial State x(0)

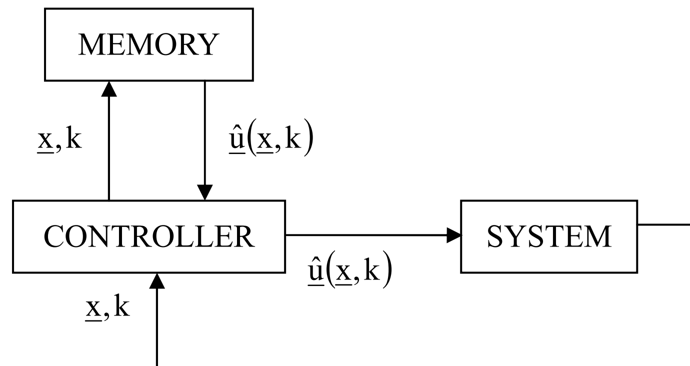

Figure 3.3 A Controller Based on Retrieving the Results of the Dynamic Programming Computation from Memory

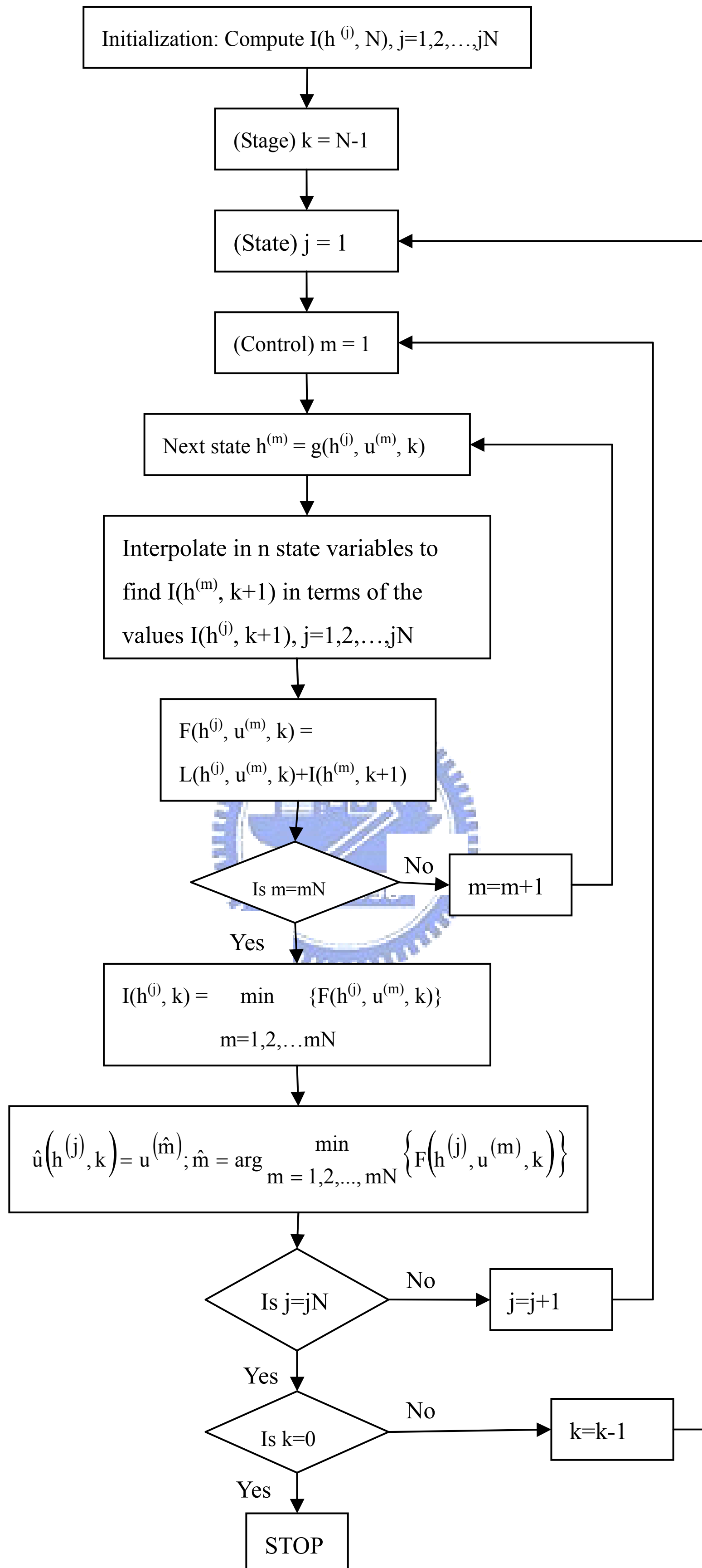

Figure 3.4 Program Flowchart of Dynamic Programming

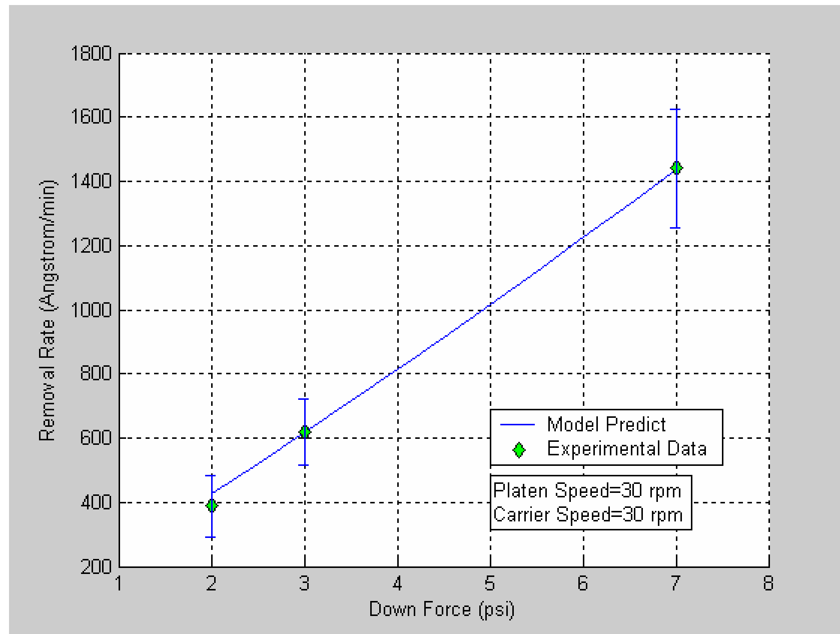

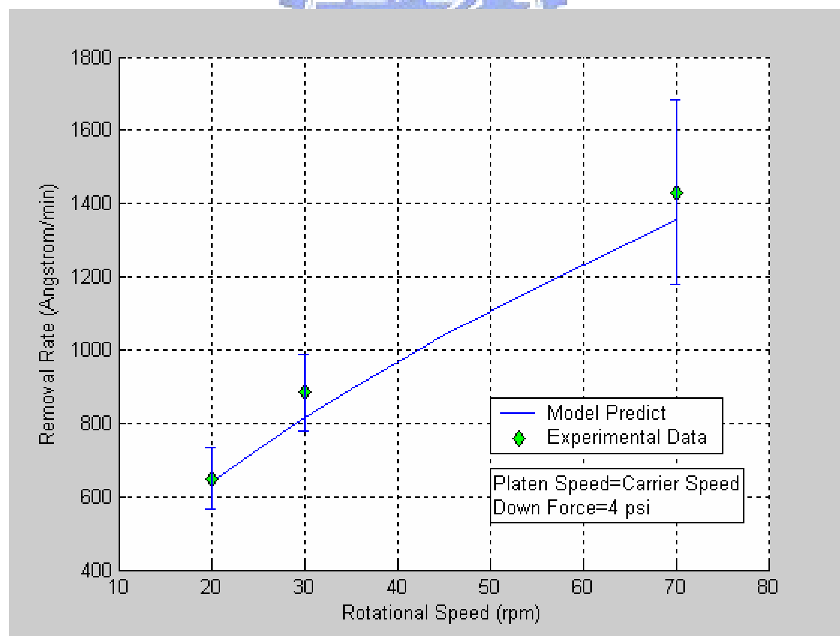

Figure 3.5 The Model Prediction and Experimental Observations of the Effects of the Down Force and Rotational Speed for SiO_2 Blanket Wafer

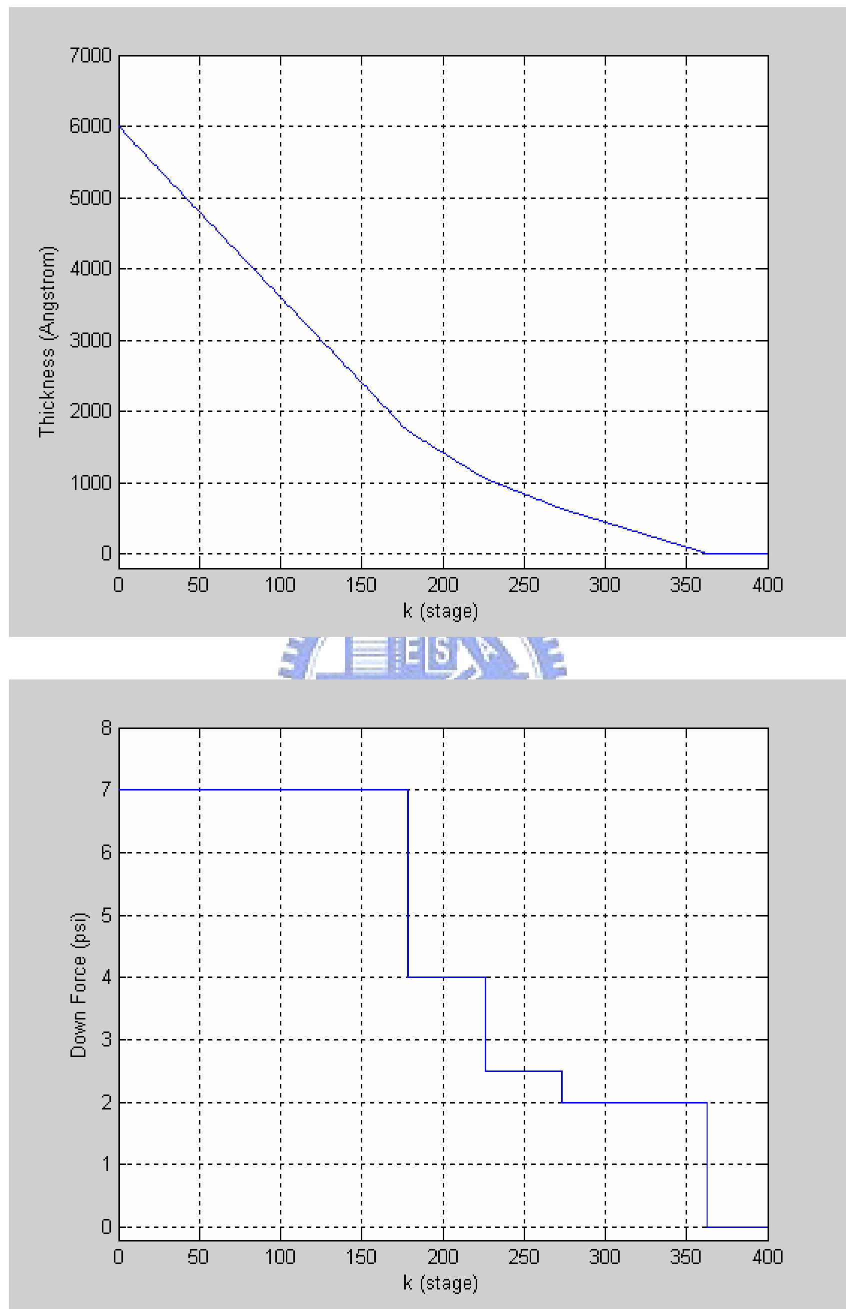

Figure 3.6 The Simulation Result of SiO_2 Blanket Wafer when the Down Force as the Variable Input

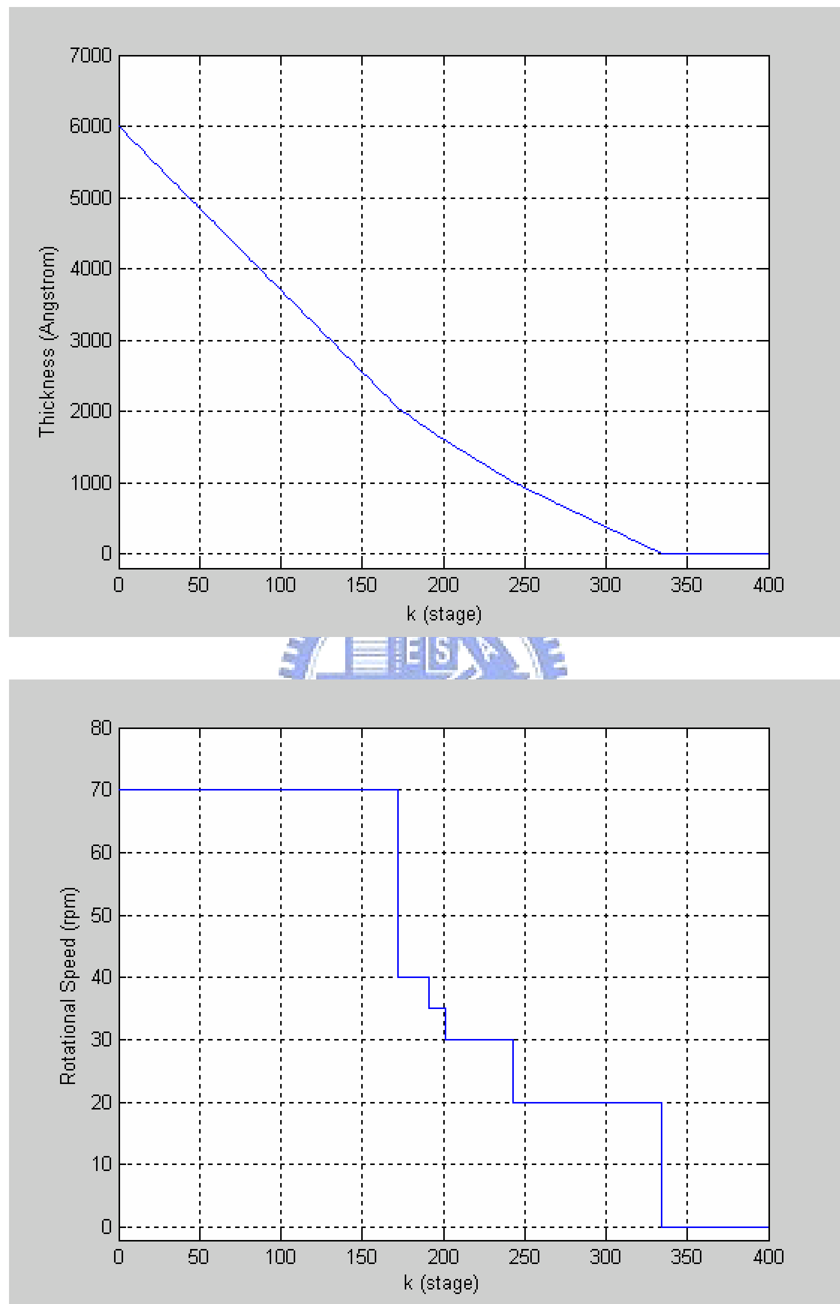

Figure 3.7 The Simulation Result of SiO_2 Blanket Wafer when the Rotational Speed as the Variable Input

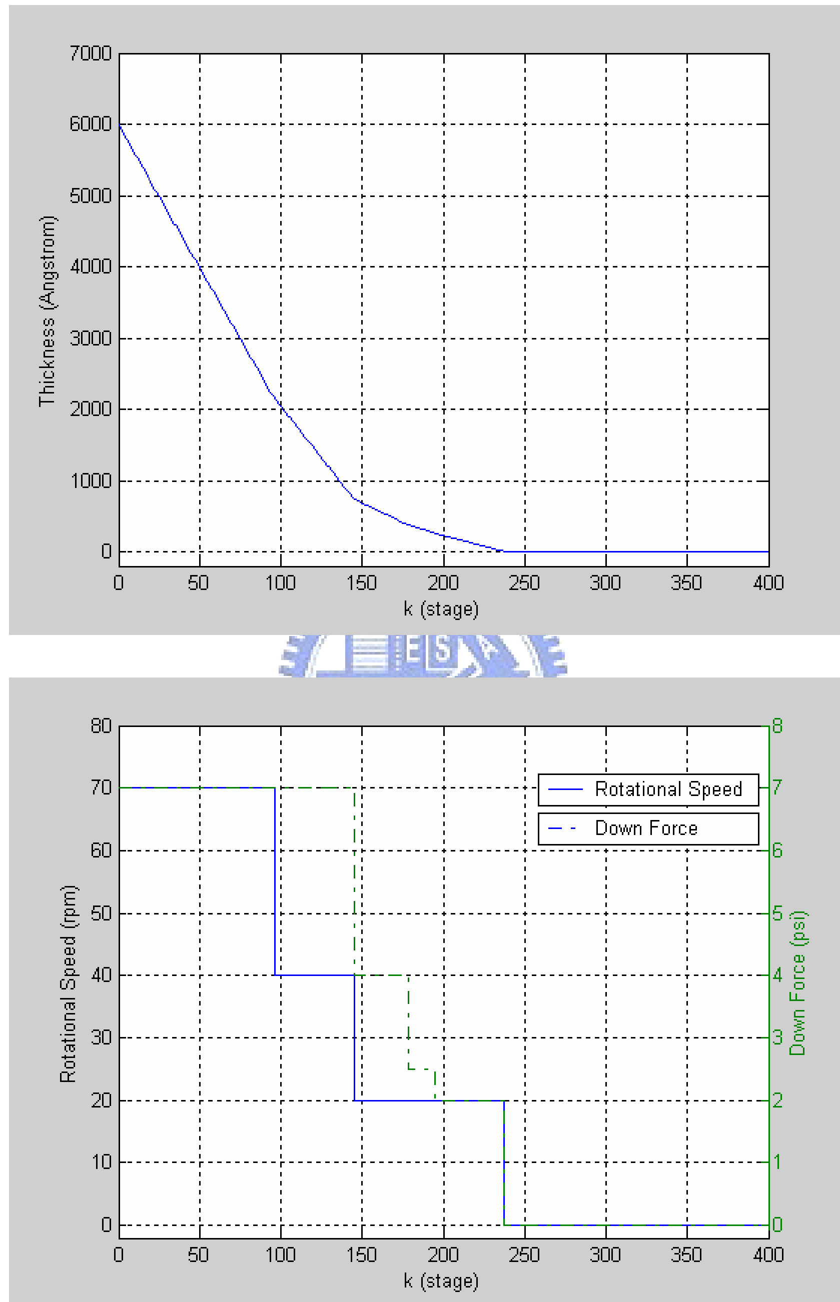

Figure 3.8 The Simulation Result of SiO_2 Blanket Wafer when the Rotational Speed and Down Force as the Variable Inputs Simultaneously

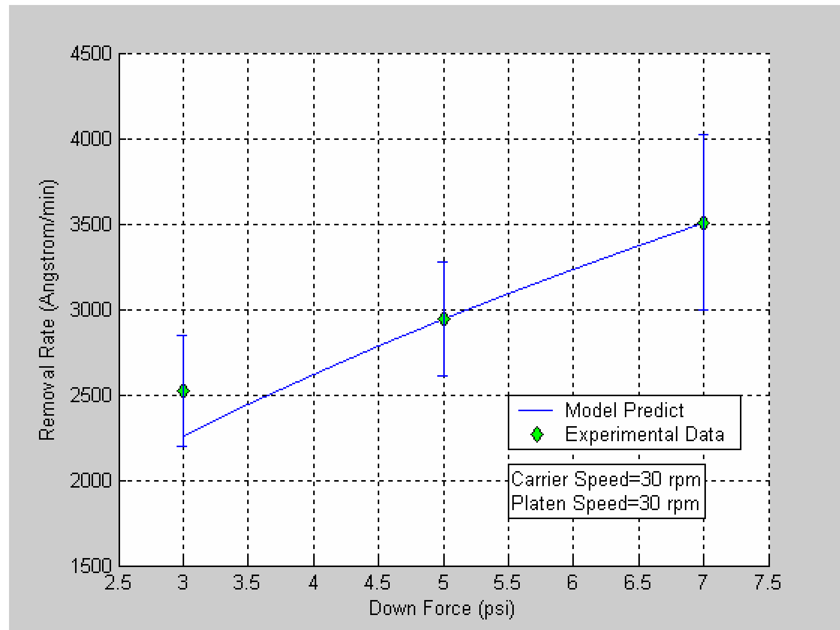

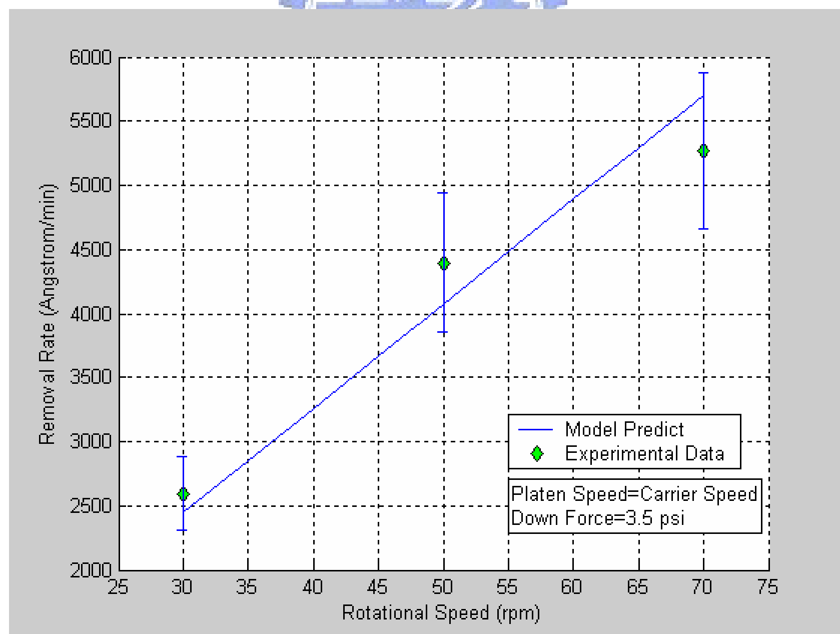

Figure 3.9 The Model Prediction and Experimental Observations of the Effects of the Down Force and Rotational Speed for Cu Blanket Wafer

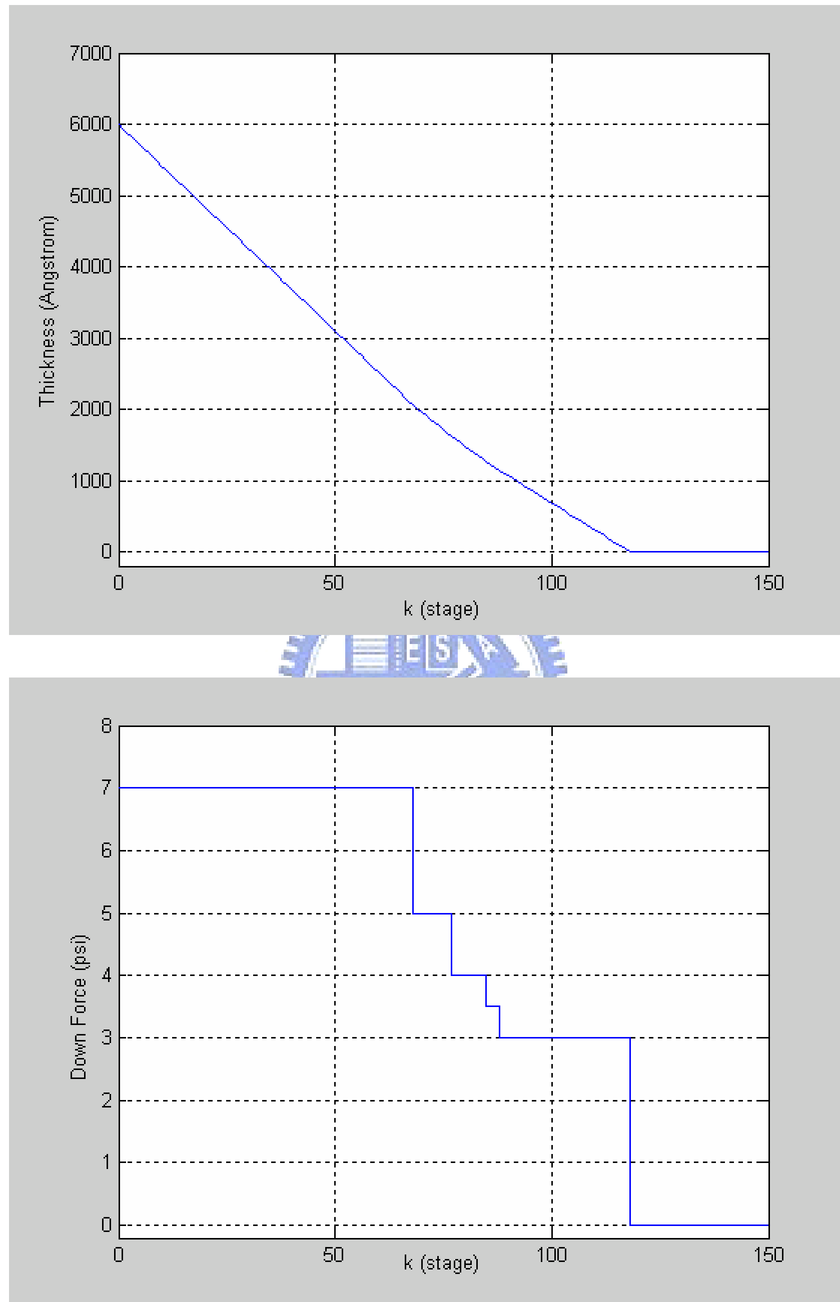

Figure 3.10 The Simulation Result of Cu Blanket Wafer when the Down Force as the Variable Input

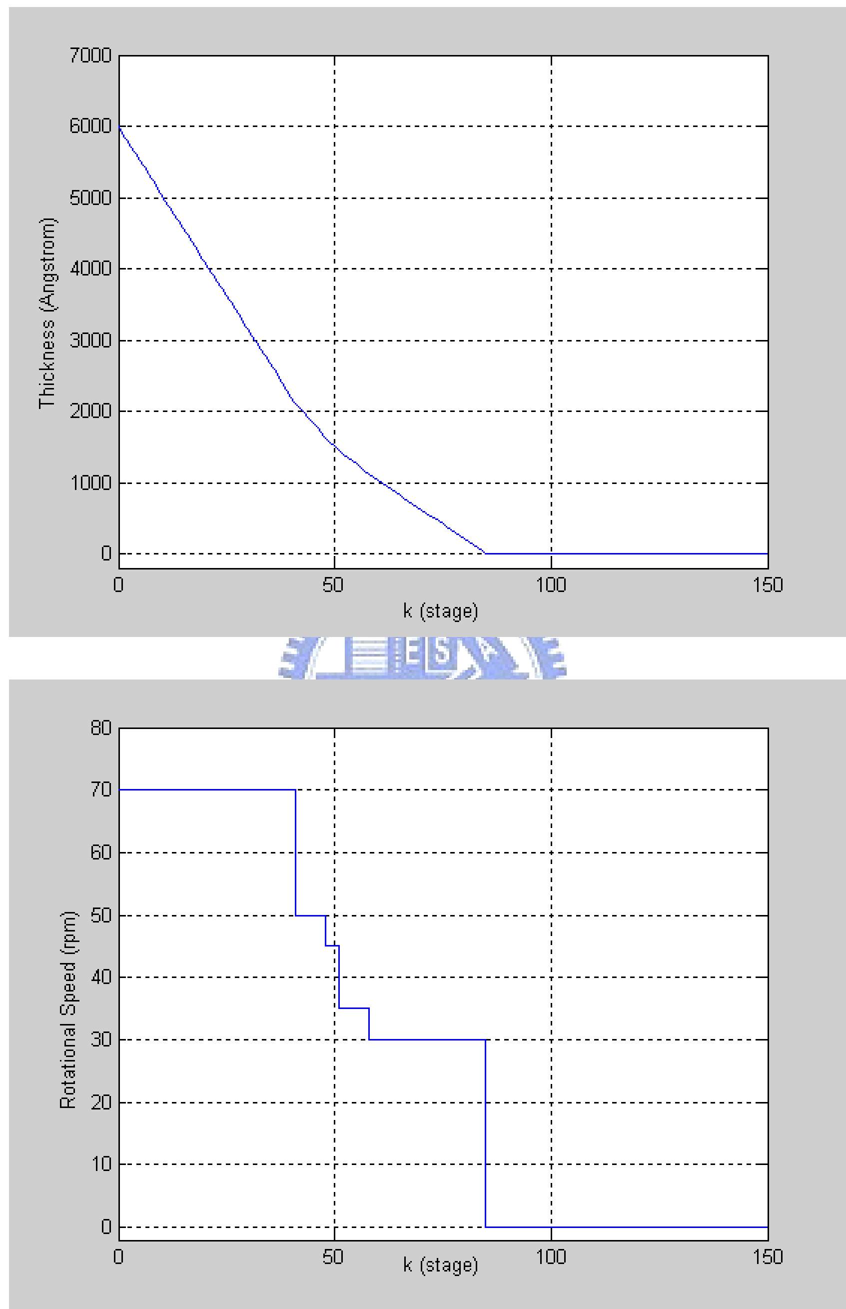

Figure 3.11 The Simulation Result of Cu Blanket Wafer when the Rotational Speed as the Variable Input

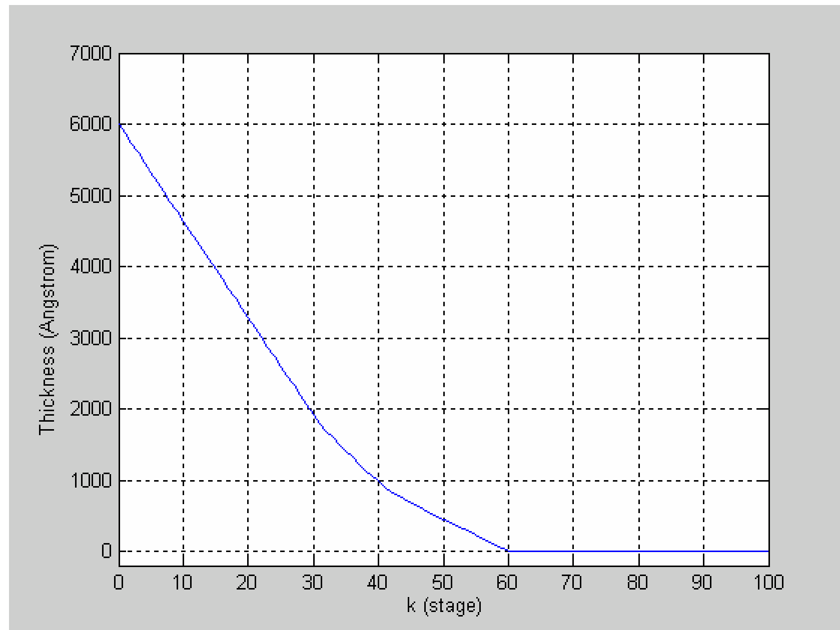

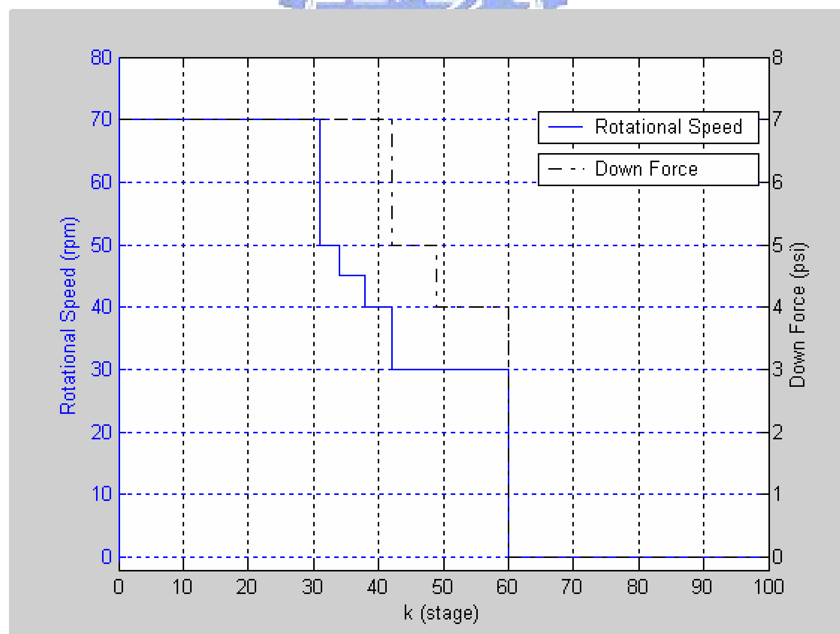

Figure 3.12 The Simulation Result of Cu Blanket Wafer when the Rotational Speed and Down Force as the Variable Inputs Simultaneously

(a)

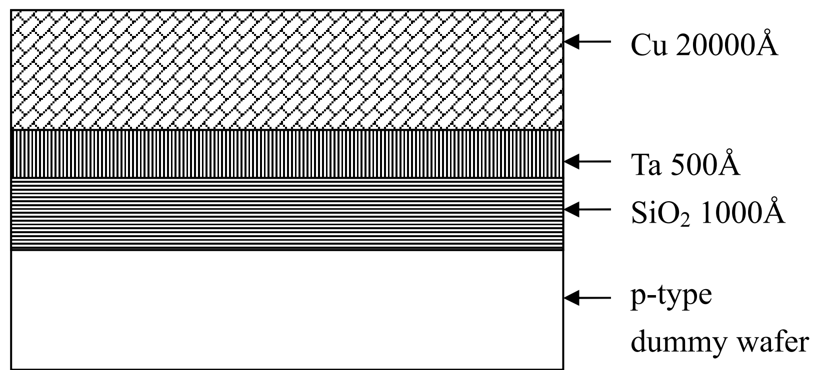

(b)

Figure 4.1 (a) The Structure of SiO_2 Blanket Wafer (b) the Structure of Cu Blanket Wafer

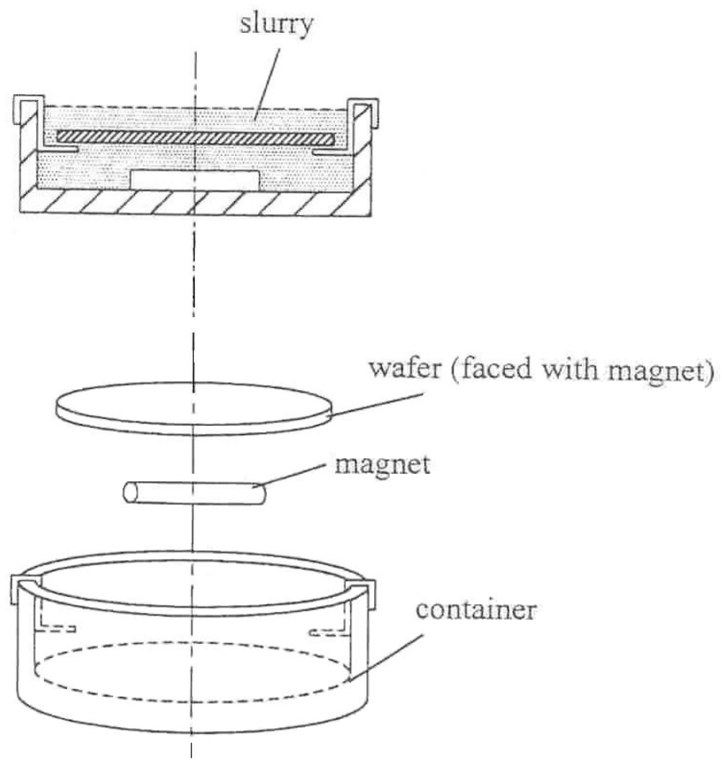

Figure 4.2 The Assembly of the Experiment for Static Etching [16]

1896

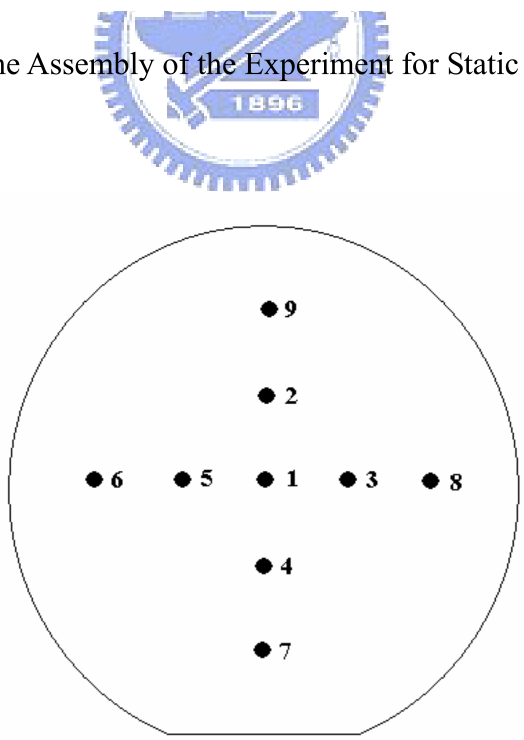

Figure 4.3 9 Points of Thickness Measurement

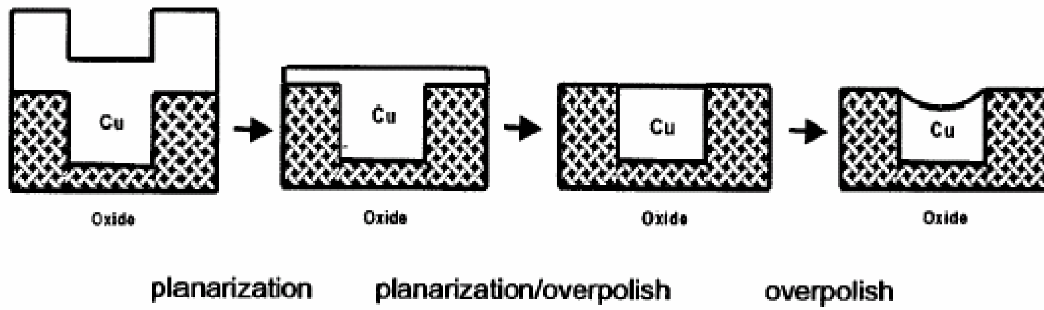

Figure 5.1 Typical Three-Step Procedure in Cu CMP: Planarization, Planarization/Overpolish, and Overpolish [28]

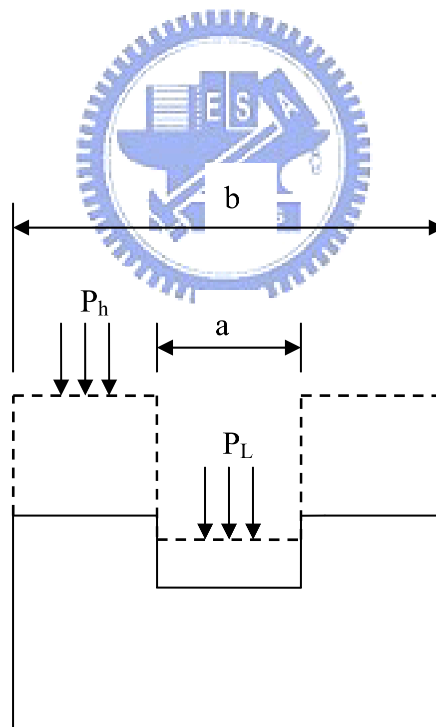

Figure 5.2 Schematic Picture of the Model

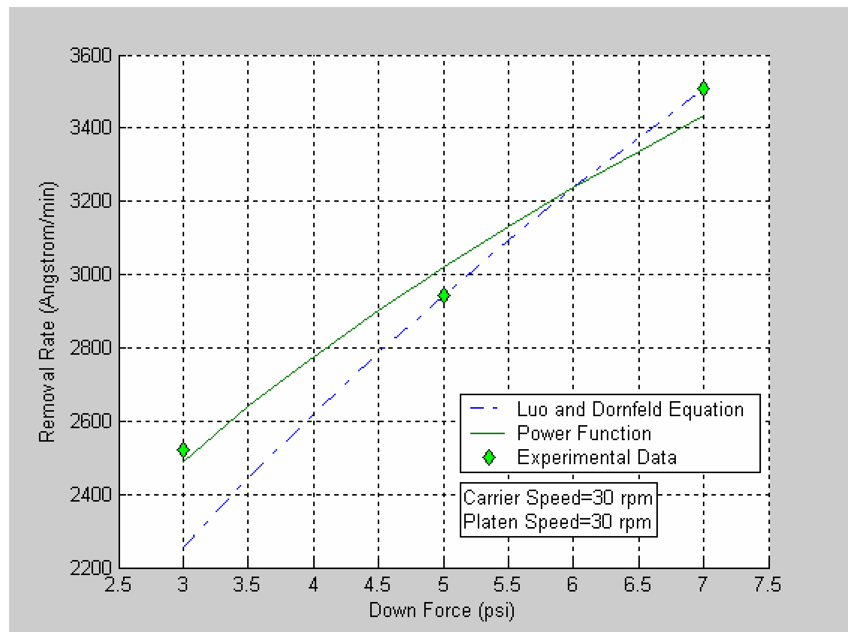

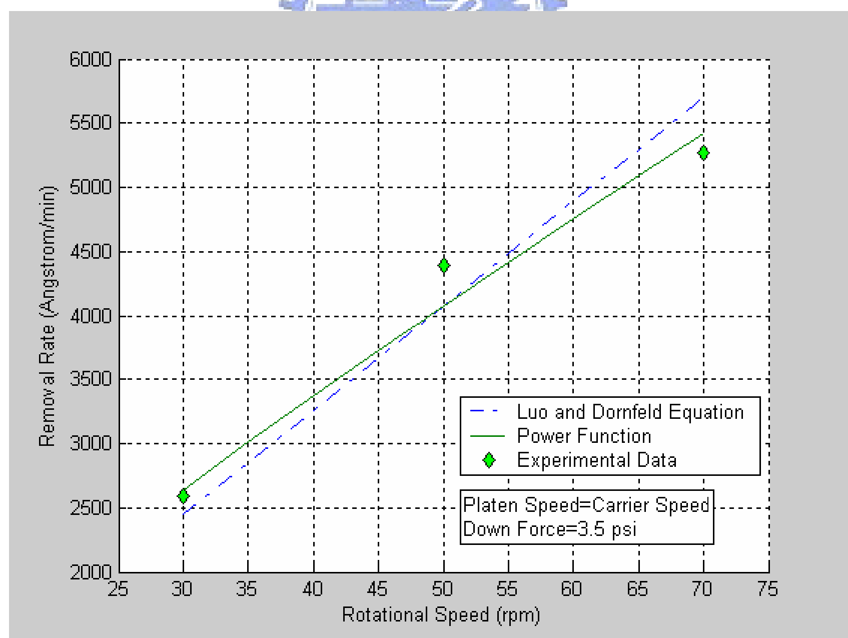

Figure 5.3 Comparison between Luo and Dornfeld Equation and Power Function Fit for Experimental Cu Blanket Wafer Removal Rate

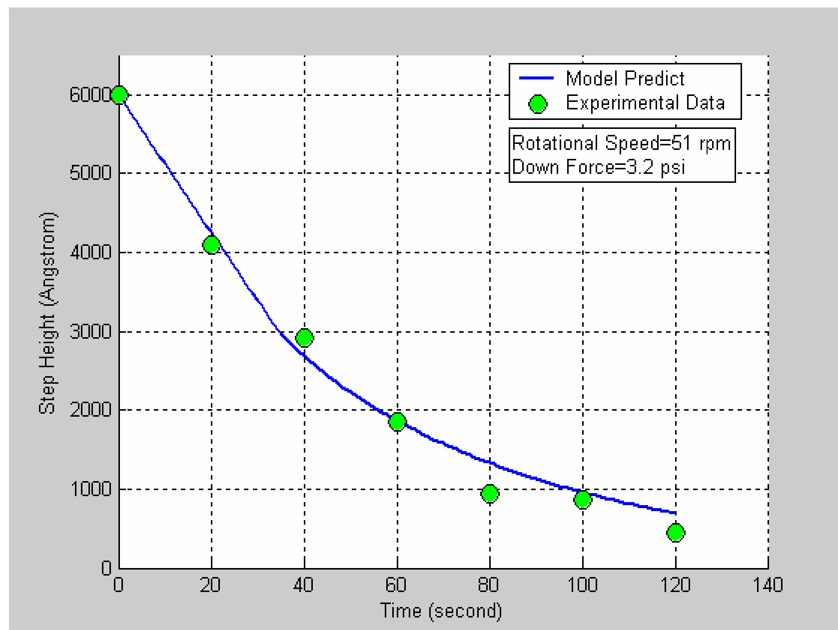

Figure 5.4 Model Prediction Compared with Experimental Data from Stavreva [22] for Step Height versus Polishing Time

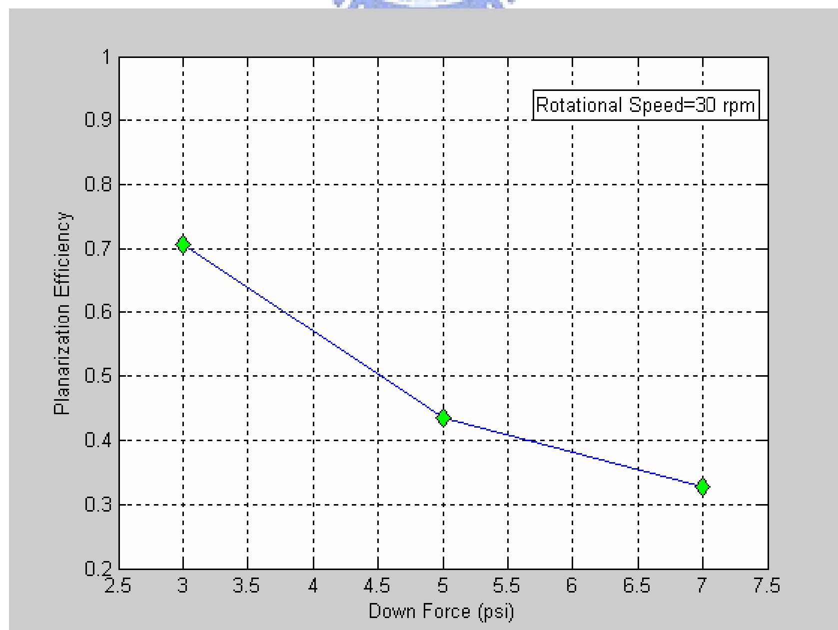

Figure 5.5 Planarization Efficiency versus Down Force

Reference:

[1] Y. Hayashi, et al., "Ammonium-salt-added silica slurry for the chemical mechanical polishing of the interlayer dielectric film panarization in ULSI's," *J. Appl. Phys.*, vol. 34, no.2B, pp. 1037-1042, 1995.

[2] C.K. Hu and J.M.E. Harper, "Copper interconnections and reliability," *Materials Chemistry and Physic*., vol. 52, pp. 5-16, 1998.

[3] F. Preston, "The theory and design of plate glass polishing machines," *J. Soc. Glass Technol*., vol. 11, pp. 214-256, 1927.

[4] F. Zhang, A. A. Busnaina, J. Feng, and M. A. Fury, "Particle adhesion force in CMP and subsequent cleaning process," in *Pro. Fourth Int. Chemical-Mechanical Planarization for ULSI Multilevel Interconnection Conf.*, Santa Clara, CA, Feb. 11-12, 1999, pp. 61-64.

[5] W. T. Tseng and Y. L. Wang, "Re-examination of pressure and speed dependences of removal rate during the chemical-mechanical polishing processes," *J.Electrochem. Soc.*, **144**, 1121, 1997.

[6] B. Zhao and F. G. Shi, "Chemical mechanical polishing in IC processes：New fundamental insights," in *Pro. Fourth Int. Chemical-Mechanical Planarization for ULSI Multilevel Interconnection Conf.*, Santa Clara, CA, Feb. 11-12, 1999, pp. 13-22.

[7] F. G. Shi and B. Zhao, "Modeling of chemical-mechanical polishing with soft pads," *Appl. Phys. A*, vol.67, pp. 249-252, 1998.

[8] J. Luo and D. A. Dornfeld, "Material removal mechanism in chemical mechanical polishing: Theory and modeling," *IEEE Trans. Semiconduct. Manufact.*, vol. 14, pp. 112-113, May 2001.

[9] Jian-Bin Chiu, Cheng-Ching Yu and Shih-Haur Shen, “Application of soft landing to the process control of chemical mechanical polishing,” *Microelectronic Engineering*, vol. 65, pp. 345-356, March 2003.

[10] K. Wijekoon, S. Tsai, M. Chandrachood, B. Brown, F. Redeker, S. Nanjangud, G. Amico, “Multi-Step Approach to Copper CMP Development,” SEMI/Japan Technical Symposium(1998)

[11] J. Luo and D. A. Dornfeld, “Effects of Abrasive Size Distribution in Chemical Mechanical Planarization: Modeling and Verification,” *IEEE Trans. Semiconduct. Manufact.*, vol. 16, pp. 469-476, August 2003.

[12] Jian-Bin Chiu, Cheng-Ching Yu and Shih-Haur Shen, “Robust operation of copper chemical mechanical polishing,” *Microelectronic Engineering*, vol. 65, pp. 61-75, March 2003.

[13] Kaufman, F. B., et al., “Chemical-Mechanical Polishing for Fabricating Patterned W Metal Features as Chip Interconnects,” *J. Electrochem. Soc.*, vol. 138, no.11, pp. 3460-3464, November 1991.

[14] Robert E. Larson and John L. Casti, “Principles of dynamic programming,” Marcel Dekker, 1978

[15] Frank L. Lewis and Vassilis L. Syrmos, “Optimal control,” John Wiley & Sons, 2nd 1995.

[16] 陳俊達, “銅膜之化學機械研磨製程應力作用對磨潤化學反應速率之影響,” 國立成功大學機械研究所, 2000.

[17] 劉耿銘, “銅薄膜之化學機械研磨之研究,” 國立交通大學電子研究所, 2000.

[18] 黃嘉雯, “研磨粉體對二氧化矽薄膜之化學機械研磨特性研究,” 國立交通大學材料科學與工程研究所, 1997.

[19] 蔡宏營,“化學機械平坦化基於材料移除與運動學之不均勻性分析,”國立清華大學動力機械工程研究所, 1999.

[20] J.M. Steigerwald, S.P. Murarka, D.J. Duquette and R.J. Gutmann, “Surface layer formation during the chemical mechanical polishing of copper thin films,” *Mat. Res. Soc. Symp. Proc.*, vol. 337, pp. 133-138, 1994.

[21] J.M. Steigerwald, R. Zirpoli, S.P. Murarka, D. Price and R.J. Gutmann, “Pattern geometry effects in chemical-mechanical polishing of inlaid copper structures,” *J. Electrochem. Soc.*, vol. 140, no. 10, pp. 2842-2848, October 1994.

[22] Z. Stavreva, “Chemical-mechanical polishing of copper for interconnect formation,” *Microelectronic Engineering*, vol. 33, pp. 249-257, 1997.

[23] Z. Stavreva, “Chemical mechanical polishing of copper for multilevel metallization,” *Applied Surface Science*, vol. 91, pp. 192-196, 1995.

[24] Dar-Zen Chen and Bor-Shin Lee, “Pattern planarization model of chemical mechanical polishing,” *J. Electrochem. Soc.*, vol. 146, no. 2, pp. 744-748, 1999.

[25] Dar-Zen Chen and Bor-Shin Lee, “Parameter analysis of chemical mechanical polishing: an investigation based on the pattern planarization model,” *J. Electrochem. Soc.*, vol. 146, no. 9, pp. 3420-3424, 1999.

[26] Guanghui Fu and Abhijit Chandra, “An analytical dishing and step height reduction model for Chemical mechanical planarization (CMP),” *IEEE Trans. Semiconduct. Manufact.*, vol. 16, no. 3, pp. 477-485, August 2003.

[27] D. Okumu Ouma, Duane S. Boning, James E. Chung, William G. Easter, Vivek Saxena, Sudhanshu Misra and Annette Crevasse, “Characterization and modeling of oxide chemical-mechanical polishing using planarization length and pattern density concepts,” *IEEE Trans. Semiconduct. Manufact.*, vol. 15, no. 2, pp. 232-244, May 2002.

[28] Jian-Bin Chiu, An-Jhih Su, Cheng-Ching Yu and Shih-Haur Shenc, "Planarization strategy of Cu CMP: interaction between plated copper thickness and removal rate," *J. Electrochem. Soc.*, vol. 151, pp. G217-G222, 2004.

[29] Ravi Saxena, Dipto G. Thakurta, Ronald J. Gutmann and William N. Gill, "A feature scale model for chemical mechanical planarization of damascene strucrures," *Thin Solid Films*., vol. 499, pp. 192-206, 2004.

[30] Jiun-Yu Lai, Nannaji Saka and Jung-Hoon Chun, "Evolution of copper-oxide damascene Structure in chemical mechanical polishing: copper dishing and oxide erosion," *J. Electrochem. Soc.*, vol. 149, pp. G41-G50, 2002.

[31] Viet H. Nguyen, Roel Daamen, Herma van Kranenburg, Peter van der Velden and Pierre H. Woerlee, "A physical model for dishing during metal CMP," *J. Electrochem. Soc.*, vol. 150, pp. G689-G693, 2003.